AIChE
JOURNAL

## REVIEW ARTICLE

### Transport Phenomena and Fluid Mechanics

# Impinging jet mixers: A review of their mixing characteristics, performance considerations, and applications

Cedric Devos[1] | Saikat Mukherjee[1] | Pavan Inguva[1] | Shalini Singh[1] |
Yi Wei[2] | Sandip Mondal[3] | Huiwen Yu[1] | George Barbastathis[2,3] |
Torsten Stelzer[1,4,5] | Richard D. Braatz[1] | Allan S. Myerson[1]

[1]Department of Chemical Engineering,
Massachusetts Institute of Technology,
Cambridge, Massachusetts

[2]Department of Mechanical Engineering,
Massachusetts Institute of Technology,
Cambridge, Massachusetts

[3]Singapore-MIT Alliance for Research and
Technology (SMART) Centre, Singapore

[4]Department of Pharmaceutical Sciences,
School of Pharmacy, University of Puerto
Rico - Medical Sciences Campus, San Juan,
Puerto Rico

[5]Crystallization Design Institute, Molecular
Sciences Research Center, University of
Puerto Rico, San Juan, Puerto Rico

**Correspondence**
Allan S. Myerson, Department of Chemical
Engineering, Massachusetts Institute of
Technology, Cambridge, MA 02139, USA.
Email: myerson@mit.edu

**Funding information**
U.S. Food and Drug Administration,
Grant/Award Number: 75F40122C00200

## Abstract

Optimal control over fast chemical processes hinges on the achievement of rapid and effective mixing. Impinging jet mixers are a unique class of passive mixing devices renowned for their exceptional ability to achieve rapid mixing at micro-length scales, whilst offering the possibility of a high throughput. Comprising of two co-linear jets flowing in opposite directions and colliding with each other within a small (usually confined) volume, these devices effectively intensify various mixing-controlled processes in a reproducible manner. Impinging jet mixers find extensive use in both the chemical and pharmaceutical industry for a plethora of applications, such as reaction injection molding and precipitation processes. This review provides an overview of research related to impinging jet mixers, with an emphasis on the mixing characteristics and the influence of design and process parameters on the mixing performance. Lastly, specific applications for which these devices are exceptionally suited are discussed.

### KEYWORDS

colliding jets mixing, confined impinging jets, flash nanoprecipitation, impingement, impinging jet mixer, micromixing, nanoparticles, reaction injection molding, Reynolds number

## 1 | INTRODUCTION

Impinging jet mixers (IJMs) represent a class of mixing equipment in which two liquid co-linear jets collide at high velocities within a small volume. Renowned for their superior performance over conventional mixing equipment (e.g., stirred tanks, static mixers, microfluidic mixers), IJMs have garnered considerable attention, see further in Figure 2. As the significance of IJMs continues to grow, there is a need for a thorough literature review. This review delves into the extensive research on IJMs, focusing on their mixing characteristics,

operational performance considerations, and applications where they have demonstrated their superiority.

Despite the pivotal role of IJMs across various fields, comprehensive reviews on the subject have been notably scarce.[1,2] Related works, such as Tamir and Kitron's 1987 review on impinging jets for gas-solid operations,[3] Tamir's book from 1994 on impinging stream reactors for intensifying multiphase transfer processes for heterogeneous systems,[4] and Tamir et al.'s review on impinging jet absorbers from 1990,[5] have had a distinct focus on applications. Transferring these discussions about contacting of immiscible liquids to IJMs for mixing of miscible liquids is not straightforward as the mechanisms governing mixing differ from those involved in interphase processes.[6] Santos and Sultan's 2013 specialized review, although valuable, focused on mixing in micro- or milliliter volume jet reactors, but its brevity limited its comprehensiveness.[2] Similarly, another concise review about IJMs for controlled synthesis of nanomaterials was published in 2020 by Abiev.[1] Here we adopt a different perspective by providing a comprehensive summary of the substantial research efforts dedicated to unraveling the intricacies of IJMs' mixing over the past four decades.[7] Comprehending the IJMs' mixing dynamics is important for leveraging their full potential across diverse applications, including both liquid and particulate processing.

## 1.1 | The need for rapid mixing in chemical processes

Numerous chemical processes require the fast and effective mixing of two incoming streams to ensure thorough homogenization of concentration, phase, and/or temperature.[6] Examples abound in applications such as polymerization[8–11] and precipitation/crystallization processes.[12–21] The importance of mixing becomes particularly pronounced when the process kinetics are faster than the mixing time.[22,23] In these instances, the speed of mixing directly impacts the final product properties,[23] including the homogeneity and presence of byproducts in liquid products, as well as characteristics such as the particle size distribution in solid products.

To assess the impact of mixing on the process, the turbulent Damköhler number (Da) can be defined as a competition between the characteristic reaction time ($\tau_{\text{reaction}}$, s) and the mixing time ($\tau_{\text{mixing}}$, s),

$$\text{Da} = \frac{\tau_{\text{mixing}}}{\tau_{\text{reaction}}}. \tag{1}$$

Based on this definition of the Damköhler number, the regime through which chemical processes proceed can be classified into three different categories[24]:

- $\text{Da} \ll 1$, reaction-controlled regime: the mixing occurs significantly faster than the reaction, such that the effective rate is purely controlled by the intrinsic reaction rate. The concentration field is homogeneous when reaction takes place.[25]
- $\text{Da} \approx 1$, mixing-controlled regime: the characteristic mixing and reaction time are of the same order of magnitude, such that

reaction and mixing are competing. The effective rate is lower than the intrinsic reaction rate.[25]
- $\text{Da} \gg 1$, instantaneous regime: the reaction rate is fast and the effective rate is controlled by the degree of mixing. The chemical reaction only takes place in the local zones where mixing has occurred.[25]

The influence of mixing on a reaction is negligible only when Da is significantly smaller than 1.[26] In processes where the mixing time is a concern in conventional equipment, IJMs prove to be highly effective tools for shifting the process into the reaction-controlled regime.[26]

## 1.2 | IJMs: a solution to mixing challenges

IJMs are composed of two co-linear fluid jets exiting a nozzle or orifice at high velocities (in the range of 1–100 m/s[27,28]) travelling toward an impingement point where they collide with one another. The flow is then forced to accelerate orthogonally outwards, resulting in unparalleled fast mixing (in the order of ms[29,30]). This configuration creates a zone characterized by extremely high energy dissipation rates (in some extreme cases even reaching $10^5$ W/kg[29]) which the process streams cannot bypass,[29] without the use of any movable mechanical parts. Typically, high energy dissipation rates lead to a reduction in the mixing time ($\tau_{\text{mixing}}$), thereby decreasing Da. IJMs offer the advantage of a high throughput (up to 2–4 L/min[1]) in a cost-effective setup,[15,31] which makes them suitable when the influence of mixing on scale-up must be minimized,[30,32] an imperative consideration for many industrial applications.[33] An IJM represented as a unit operation is shown in Figure 1.

IJMs have been a staple technology for several decades, with roots tracing back to the 1950s. For instance, Carver et al.[34] secured a
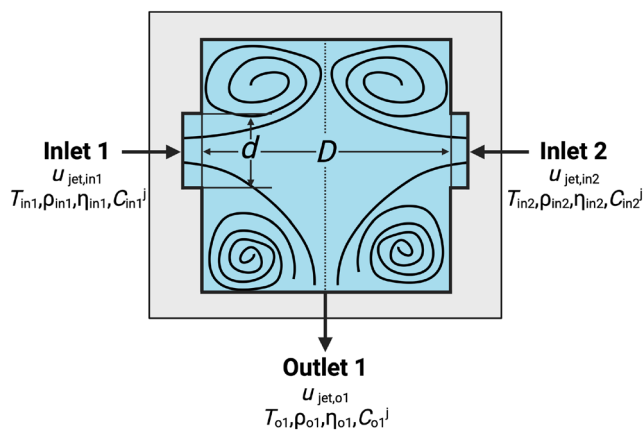


**FIGURE 1** Schematic representation of impinging jet mixers (IJMs) as a unit operation with two inlet and one outlet stream (s), characterized by a jet velocity ($u_{\text{jet}}$, m/s), density ($\rho$, kg/m$^3$), viscosity ($\eta$, kg/m s), and concentration ($c^j$, units as per convention). Two critical geometric parameters are indicated: the nozzle diameter ($d$, m) and the chamber diameter ($D$, m). Created with BioRender.com.
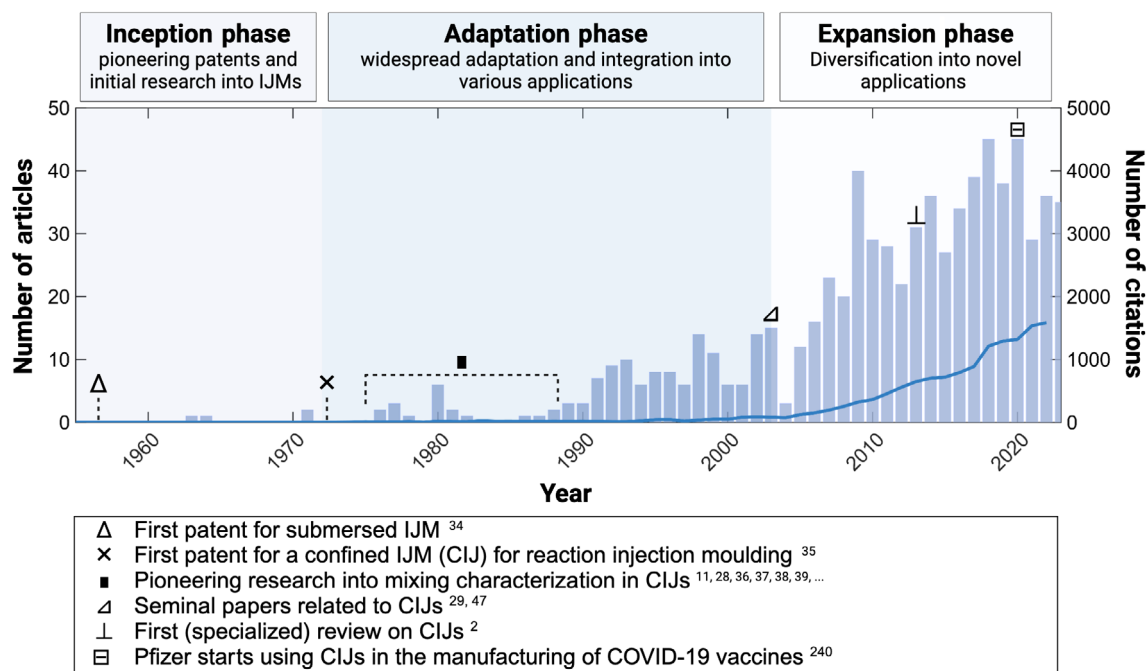
**FIGURE 2** The number of publications (bars, left y-axis) and their corresponding citations (solid line, right y-axis) related to impinging jet mixers (IJMs). Some notable contributions (e.g., References 2,29,34,35,47, and 240), discussed in Section 1.2, are highlighted with symbols. The timeline is divided into three periods based on publication and citation counts. The data, sourced from Web of Science,[7] was obtained using the search query: ("confined impinging jet" OR "two-impinging jet" OR "dual impinging jet" OR "dual impinging jets" OR "opposed jet mixer" OR "opposed jet mixing" OR "opposed jets mixer" OR "impingement mixer" OR "impinging sheets" OR "impinging-jets" OR "impinging stream reactor" OR "impinging stream mixer" OR "impingement mixer" OR "two-impinging-jets" OR "two-impinging-jet" OR "opposed-jet mixer" OR "opposed-jets mixer" OR "impingement mixing" OR "impinging jet crystallizer" OR "impinging jet contactor") NOT (cooling OR heat transfer OR medical OR erosion OR cyclones OR spray OR flame). Created with BioRender.com.

patent in 1956 for an apparatus designed for mixing through "opposed jet discharge" within a designated contacting zone. Another patent for a different IJM-type apparatus was awarded in 1972 to Keuerleber et al. .[35] Pioneering research characterizing mixing within IJMs,* particularly confined IJMs, was led by groups such as those headed by Suh,[11,36,42,43] Macosko,[14,28,38,41,44,45] and Kirwan.[20,23,46] Prud'homme's contributions furthered the understanding and application of confined IJMs (CIJs).[29,47] More recent investigations into mixing within IJMs have been conducted by Fox,[33,48–52] Marchisio,[48,49,53–58] Lopes and Santos,[2,8,27,59–69] and collaborators. In addition to this, a vast body of the literature referencing IJMs has been produced, see Figure 2, with an average of around 40 papers per year in recent years.[7] A substantial portion of these publications showcase applications of IJMs,[7] reflecting their increasing relevance and impact in various fields.

## 1.3 | Mixing in IJMs

Comprehending the mixing dynamics arising from the direct collision of two jets is essential for utilizing IJMs effectively. Mixing phenomena in IJMs are most accurately described through the systems approach of the macro-micromixing theory. This theoretical framework divides the mixing process of two miscible fluids into three distinct length scales: micro-, meso-, and macromixing,[70] as illustrated for IJMs in Figure 3. The larger scales of mixing shape the environment in which the smaller scales of mixing take place.

Macromixing involves the bulk mixing at the largest scales of motion, for example, spanning the size of an entire batch reactor.[6] Mesomixing serves as the intermediate scale of mixing between the macro- and micro-scale and takes place in the inertial-convective subrange, see Figure 3. Micromixing occurs at the finest scales of mixing, at length scales below the Kolmogorov scale ($\lambda$, m), and involves the complete homogenization of mixtures at the molecular level.[70] A comprehensive discussion of turbulent mixing is intentionally omitted in this review as it is outside the scope, but can be found in the literature.[6,22,71] Instead, focus is directed toward elucidating specific features that are most pertinent to the understanding of mixing within IJMs.

Upon impingement of two jets some degree of turbulence is generated, giving rise to a cascade of increasingly smaller whirling fluid motions that behave coherently, called eddies, through the mesoscale who dissipate the turbulence.[6] Mesomixing can thus be considered as a mechanism of scale reduction through which eddies decrease in size and energy. The Kolmogorov length scale,

$$\lambda = \left(\frac{\upsilon^3}{\varepsilon}\right)^{1/4}, \tag{2}$$

---

*At the time more commonly referred to as "impingement mixers" (e.g., References 11,28,36–41). The term "confined impinging jet mixer" was coined by Prud'homme in 2003.[29]
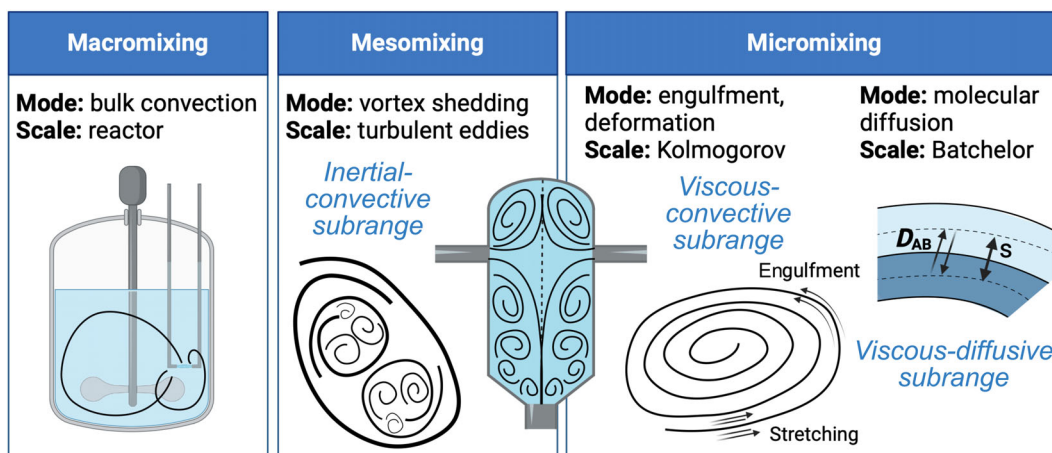
**FIGURE 3** Fluid mixing in impinging jet mixers (IJMs) at different scales within the context of the macro-micromixing theory where turbulent energy cascades from larger to smaller scales until it reaches the viscous-diffusive subrange where it is dissipated into heat. Eddies are represented as two-dimensional vortices that are shed in the inertial-convective subrange and are stretched and engulfed in the viscous-convective subrange. Adapted from Johnson and Prud'homme[29] and inspired by Baldyga and Bourne.[22] Created with BioRender.com. Copyright ©2003 American Institute of Chemical Engineers (AIChE).
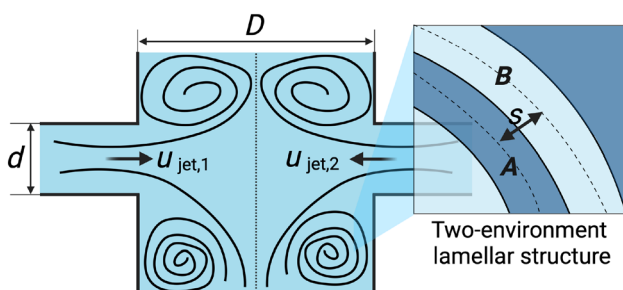


**FIGURE 4** Schematic representation of the impingement of two jets during mixing of two miscible fluids (A, B) in an impinging jet mixer (IJM) under turbulent-like conditions, and the local lamellar structure that is formed as a result. The striation thickness (s) for a mixture of two components (A-rich zones in dark blue and B-rich zones in light blue, representing the lamellae[241]) is indicated. Adapted from Lee et al. [28] and inspired from Baldyga and Bourne.[39] Created with BioRender.com. Copyright ©1980 Society of Plastics Engineers, Inc.

represents the size of the smallest eddies,[6] with $\varepsilon$ being the energy dissipation rate (W/kg) and $\upsilon$ the kinematic viscosity (m²/s). When mixing fluids with dissimilar viscosities, $\lambda$ (m) is often estimated using the kinematic viscosity of the outlet stream ($\upsilon_o$ in Figure 4).[29,72] Below the Kolmogorov microscale, the fluids continue to deform through stretching and engulfment, which results in the formation of a heterogeneous lamellar structure,[6,73,74] which is schematically shown in Figure 4. The final stage of micromixing is the diffusion of the two components into each other.

The striation thickness (s, m) serves as a metric for the microscale thickness of the lamellae, defined as half the sum of the lamellae thickness of the two components.[73] As mixing improves, s decreases, thereby reducing the distance reagents must diffuse through before reaction can occur.[28,73] In laminar flow, a mixing time can be defined by

$$\tau_{\text{mixing}} = \frac{s^2}{D_{AB}}, \tag{3}$$

with $D_{AB}$ being the molecular diffusivity (m²/s).[6,72]

While mixing in turbulent flow is conceptually similar,[6] albeit across a larger array of length scales, the concept of striation thickness does not capture the entire complexity, such that Equation (3) is not valid. A number of mixing times have been proposed in the literature, for example, assuming that the material does not diffuse before reaching the smallest eddy ($\lambda$) and ignoring the stretching and folding at the microscale results in Reference 6

$$\tau_{\text{mixing}} \propto \frac{\lambda^2}{\text{diffusivity}}. \tag{4}$$

The model proposed by Bourne and Baldyga[6,75] relates the turbulent micromixing time to the energy dissipation rate,

$$\tau_{\text{mixing}} \propto \left(\frac{\upsilon}{\varepsilon}\right)^{1/2}, \tag{5}$$

by assuming that fine-scale engulfment is the time-limiting step.

Corrsin[6,76] proposed a mixing time as the sum of the time for scale reduction from the inertial-convective (i.e., mesomixing) scale to the Kolmogorov scale and the time required for viscous dissipation below the Kolmogorov scale,

$$\tau_{\text{mixing}} \propto \underbrace{2\left(\frac{L_s^2}{\varepsilon}\right)^{1/3}}_{\text{Mesomixing Control}} + \underbrace{\frac{1}{2}\left(\frac{\upsilon}{\varepsilon}\right)^{1/2}\ln \text{Sc}}_{\text{Micromixing Control}}, \tag{6}$$

with $L_s$ being the initial segregation thickness (m) and Sc being the Schmidt number. The Schmidt number is defined as the ratio of

the momentum diffusivity (i.e., the kinematic viscosity) and the molecular diffusivity.[6]

Given the small volume (in the micro- and mesoscale) in which mixing in IJMs occurs, the importance of macromixing to the overall mixing performance is negligible. Consequently, impinging jet mixing is determined by mesoscale and most importantly micromixing processes below the Kolmogorov scale.[26,29] Considering that chemical processes including chemical reactions are governed by the local flow topology and occur inherently at the microscale,[6] the significance of optimizing micromixing becomes evident.

## 1.4 | Content structure

To further discuss the topic, this article is structured as follows: Section 2 delves into the design and operational parameters of IJMs, alongside an overview of related mixing equipment. Section 3 covers experimental and computational approaches for mixing characterization. Section 4 discusses mixing in IJMs, followed by operational performance considerations in Section 5. Section 6 focuses on applications closely linked to IJMs. Finally, Sections 7 and 8 offer future perspectives and conclusions, respectively.

## 2 | TECHNOLOGY AND DESIGN

### 2.1 | Design parameters

IJMs can be classified into three categories based on the environment in which the jet collision occurs: submerged IJMs, free IJMs, and CIJs.

In a submerged IJM, see Figure 5A, the two jets are surrounded by a fluid that considerably affects the jets' velocity through entrainment and hinders the linear flow.[29,77] In contrast, the jets' velocity in free IJMs is unaffected by the surrounding ambient fluid.[29,77] At high Re, the impact of entrainment diminishes, and the performance of submerged IJMs approaches that of free configurations.[23] When the IJM is positioned at position $x_2$, see Figure 5A, the ratio of energy dissipation rates caused by the IJM and the impeller are about unity, whereas at positions $x_1$ and $x_3$, the ratio is orders of magnitude higher.[30]

CIJs can be considered an extension of free IJMs, see Figure 5B, in which the jets collide within a small chamber, such that the chamber walls have a strong impact on the flow hydrodynamics and mixing.[29] While the transition from free to CIJs is not necessarily well-defined, Johnson and Prud'homme showed that a shift occurs when the ratio of chamber diameter to nozzle diameter ($D/d$) falls below the range of 10–20.[29] Current literature on IJMs predominantly centers around CIJs,[7] as spearheaded by Prud'homme et al.[29,47]

Key design features are the nozzle diameter ($d$, typical values range from 0.5 to 3 mm) and the chamber diameter ($D$, typical values range from 1 to 20 mm) and, in the case of submersed IJMs, the inter-nozzle distance ($D_i$, typical values range from 1 to 20 mm with narrower spacing yielding superior results compared to wider spacing, as the latter encounters more liquid resistance[78]). Most chambers in CIJs are cylindrical,[8,28,36,79,80] although some exceptions with prismatic chambers exist,[81] with the chamber multiple usually reported as the ratio of the chamber diameter to the jet diameter ($D/d$, typical values range from 2 to 12 with larger multiples resulting in worse mixing performance, eventually converging to the level of free IJMs[29]). In those cases, the volume is determined by both the chamber diameter ($D$), chamber height ($H$), and other chamber dimensions. In CIJs, the top chamber distance, $h$ in Figure 5, may seem insignificant for mixing,[11] and some CIJs have been operated without a headspace (e.g., Reference 26). In addition, recirculation flows in the headspace
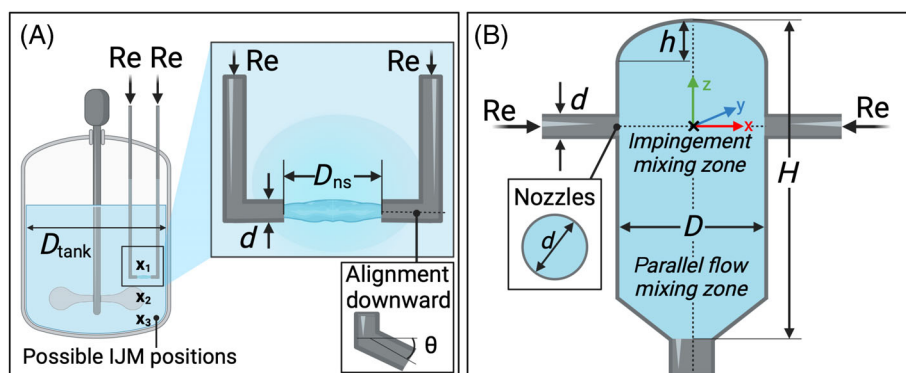


**FIGURE 5** (A) Example of a typical impinging jet mixer (IJM) submersed in a stirred tank with key dimensions indicated, such as the nozzle diameter ($d$), the internozzle separation ($D_{ns}$), and tank diameter ($D_{tank}$, m). Three possible IJM positions are indicated with $x$. An example of a jet with different alignment angle ($\theta$) is also shown. (B) Example of a typical confined impinging jet mixer (CIJ) geometry with key dimensions indicated, such as the nozzle diameter ($d$), chamber diameter ($D$), chamber height ($H$), and hemispheric dome height ($h$, m). The hemispheric dome is the dome type most associated with CIJs, but other domes have been investigated (e.g., Reference 84). This CIJ has a conical outlet configuration. The ideal impingement point is indicated with a cross. The location of the impingement mixing zone (near the impingement point) and the parallel flow mixing zone (downstream from the impingement point) are also highlighted. Axes orientation is highlighted in color. If $D/d$ is greater than 10 or 20,[29] (B) shows a free IJM. Created with BioRender.com.

may cause locally concentrated regions, which are not present in the rest of the chamber.[82] Yet, the headspace is vital for providing sufficient room for the dynamic flow behavior, see Section 4, to develop.[83] Some authors have reported on CIJs with larger dimensions (e.g., chamber diameters up to 4.5 times greater than typical, but with normal chamber multiple ratios).[84,85] The impingement point is defined as the point where the two streams collide and where the velocity magnitude reaches a minimum value.[82] Sometimes the impingement point is located slightly downstream, due to bending of the jets before impingement.[86]

Other relevant design parameters are the impingement angle ($\theta$) and the nozzle geometry characteristics. Typically, the injector nozzles of IJMs have a circular geometry and are aligned co-linearly (with $\theta = 0°$), but also upward- (against gravity, e.g., References 28,44, and 78) and downward-angled (e.g., References 26,78,85, and 87) jets have been explored to overcome the iso-momentum/iso-kinetic energy requirement,[26,27,78,88] see Section 5.

For CIJs, different mixing chamber geometries and configurations have been investigated.[29,84,88,89] Outlet shape (e.g., conical, square) has minimal impact, but outlet size can influence process performance and can aid in finalizing the mixing.[29] Variations in dome geometries (e.g., plane or hemispheric) and chamber shapes (e.g., square or round) have marginal impact on mixing when compared to parameters such as $D/d$ and $h$.[84] In some CIJs, turbulence-inducing inserts have been introduced.[88,90] However, modifying CIJs often leads to increased complexity without commensurate performance enhancements, rendering such alterations questionable.[88] This article advocates for adhering to traditional CIJ geometries.

To overcome the requirement of equal momentum of the incoming fluid streams in CIJs (see Section 5.1), while retaining the fast mixing, a four-jet version called the multi-inlet vortex mixer (MIVM) was developed, with inlet streams oriented tangentially to the inner chamber.[52] In the MIVM design, each stream independently contributes to the micromixing process, offering greater flexibility, for example, to achieve higher supersaturation or to use multiple solvent types (e.g., References 91–94). Comparable levels of turbulence can be achieved in MIVMs as in CIJs, but with the maximum mixing intensity occurring near the chamber exit.[52] Different scale MIVMs have been reported,[52,92,93] with the larger ones capable of accommodating flow rates up to 5 L/min (at Re = 100,000, see Section 2.2).[52,92]

The difference between CIJs and T-shaped jet mixers might be unclear: A key discrepancy lies in the fact that the inlet channels in T-shaped microfluidic mixers extend throughout the entire depth of the mixer, which is not the case for CIJs.[2,95] Due to the absence of a chamber for turbulence to develop in T-mixers, the resulting mixing dynamics and flow patterns are different, see Section 4.1. In addition, most T-jet mixers have square jet nozzles as opposed to the round injectors more commonly used for CIJs.[95]

Some other alternative designs departing from conventional IJM configurations have been investigated.[14,18,42,96,97] Examples include triple IJMs, where three streams collide instead of two[43,97]; a multiple (cascade) impingement device, where two streams undergo cycles of impingement, separation, and re-impingement (up to 90 times)[42]; and

a hand-held variant, called the CIJ with dilution.[14] The latter maintains similar design dimensions to typical CIJs, but relies on the use of low-friction syringe pumps connected by a metal plate, such that manual actuation is possible.[14] In this design, the outlet stream directly leaves the confinement chamber into a large dilution reservoir (which allows rapid quenching with an antisolvent).[14]

To overcome the Coandă effect, which causes fluid jets tend to attach to nearby chamber walls, a design with inlet jet nozzles elongated into the mixing chamber and a modified chamber geometry was used.[18] Another CIJ concept with adjustable inlet jets was proposed to adjust the mixing rate without changing the flow rates.[98] To improve residence time uniformity, albeit at the expense of mixing efficiency, a CIJ design featuring an axisymmetrical chamber and a circumferential rim outlet was proposed.[96] To exploit the oscillatory behavior of impinging jets, see Section 4.2, an IJM with an annular-shaped collision chamber was developed.[99] Lindrud et al. [100] obtained a patent for an active submersed IJM-configuration in a 1-L stirred tank reactor with an ultrasonic horn (preferably operated at a frequency of 20 kHz) positioned with the probe tip as close as possible to the impingement zone. By sonicating near the impingement zone, the micromixing can be improved further[100] due to higher local energy dissipation rates. Sonication has also been utilized within a CIJ for the production of nano-emulsions[101] and nanoparticles.[102] At high flow rates, the influence of sonication is expected to be negligible.[102]

## 2.2 | Operational parameters

Optimizing the mixing performance of IJMs requires the proper selection of a number of operating parameters. The dominant parameter governing the mixing process within IJMs is widely recognized to be the Reynolds number (Re), with higher Re leading to better mixing.[23,29,36,42,63–65] Reynolds numbers in the range of 250–600 are of most interest for the reaction injection moulding industry,[61,103] whereas Re from 10,000 up to 100,000 are used in nanoparticle manufacturing.[47,92,93] Reynolds numbers in IJMs are defined based on Re of the inlet,[11]

$$\text{Re} = \frac{\rho u_{\text{jet}} d}{\eta}, \tag{7}$$

with $u_{\text{jet}}$ being the superficial jet velocity (typical values ranging from 1 to 100 m/s[27,28]), $d$ being the nozzle diameter, $\rho$ being the solution density, and $\eta$ being the dynamic viscosity of the solution (Pa s). While the flow inside the tubes delivering the jets typically remains laminar, the mixing dynamics at the impingement point of the IJM can vary, ranging from laminar to fully turbulent, or falling within the transition regime.[33,50] Above a critical Reynolds number (Re$_{\text{crit}}$) the flow patterns change drastically and the mixing is improved considerably,[8,24,28,37,63,84] as discussed in Section 4.1.

When dealing with jets of differing Re, the best approach is to consider Re of the jet with the lowest value, as it ensures that Re$_{\text{crit}}$ remains similar to that of symmetric operation (provided the jets are

**TABLE 1** An overview of selected publications reporting the $Re_{crit}$ in various impinging jet mixers (IJMs), including the authors, IJM type, chamber multiple ($D/d$), chamber diameter ($D$), and the range of Re values studied. Adapted from a table reported by Fonte et al. .[8]

| Authors | IJM type | $D/d$ (–) | $D$ (mm) | Re range | $Re_{crit}$ |
|---|---|---|---|---|---|
| Tucker III and Suh[36] | Confined | 2.33 | 22.00 | 50–2000 | 140 |
| Lee et al.[28] | Confined | 3.18 | 3.18 | 50–150 | 90–150 |
| Kusch et al.[37] | Confined | 4.90 | 5.00 | 19–773 | 100–200 |
| Wood et al.[80] | Free | 10.67 | 25.40 | 60–300 | 135 |
| Johnson and Prud'homme[29] | Confined | 4.8–19 | 4.0–12.5 | 300–1000 | 90 |
| Teixeira et al.[103] | Confined | 6.66 | 10.00 | 50–600 | 50–100 |
| Santos et al.[64] | Confined | 6.66 | 10.00 | 100–500 | 120 |
| Nunes et al.[24] | Confined | 6.66 | 10.00 | 75–600 | 120 |
| Fonte et al.[8] | Confined | 6.66 | 10.00 | 50–600 | 110 |

balanced, see Section 5.1).[27] Earlier studies suggested that Re is governed by the most viscous fluid,[11] though these studies did not balance the jets.

Table 1 presents the $Re_{crit}$ values identified for IJMs in the literature.[8,24,28,29,36,37,64,80,103] For typical IJMs, the transition from laminar to more turbulent-like mixing occurs in a narrow interval of Re between 90 and 150.[8,24,28,36,37,64,80,81] When Re surpasses this critical threshold, the predominant phenomenon is the emergence of vigorously dynamic vortices, see Section 4.2, that facilitate fluid engulfment.[64]

Metzger and Kind[26] identified a Re threshold where cavitation bubbles start appearing along the core axis of vortices.[26] This transition from noncavitation to cavitation regime was observed at approximately Re $\approx 3100$ in a CIJ ($d = 0.50$ mm, $D = 2.00$ mm). Continuous vortex cavitation was noted around Re $\approx 3400$, with increasing Re intensifying cavitation with an intermediate minimum at Re $= 4200$.[26]

Recently, Hao et al. [96] showed that a sinusoidal oscillation velocity perturbation, in which both jets have the same frequency and amplitude but are 180° out of phase, can improve mixing (especially for low Re, e.g., 200) in a CIJ ($D/d = 6.6$). Similarly, results of Shi et al. [104] indicate that a periodic excitation improved mixing in a CIJ ($d = 4.20$ mm, $D = 20.08$ mm) at low and moderate Re values (100–500). Brito et al. [68] modulated the jet velocity with typical frequencies associated with certain vortices, see Section 4.2, to promote a state of resonance within a CIJ ($d = 1.5$ mm, $D = 10$ mm). Similarly, Erkoç et al. [62] studied the effect of pulsations (with a frequency multiple of the natural oscillation frequency) on mixing in a T-jet mixer.

In principle IJMs are designed for head-on impingement of two parallel jets. The momentum balance of the two jets, discussed in Section 5, is an important operational parameter that affects the mixing considerably.[8,11,24,36,66,69]

While the mixing performance of IJMs can also be influenced by operational parameters such as operating temperature and solvent choice, these factors are typically dictated by the specific requirements of the application for which the IJM is used. If there are no process constraints, increasing the temperature enhances diffusion and consequently improves mixing.[78] Moreover, the viscosity of the impinging streams can have an impact on the mixing,[24,27,29,46,80,105] as detailed in Section 5. For IJMs in submerged stirred tanks, the stirring rate of the tank impeller has an impact on the mixing conditions around the IJM. Thus, the stirred tank should be operated such that the mixing from the impeller does not disrupt the mixing at the impingement point.

The jet velocity and the pressure drop through the delivery lines determines the pump selection.[26] The pressure drop through the delivery lines can be estimated, for instance, using traditional pressure drop calculations for flow through a pipe.[26,78]

To account for the independent contributions of different streams to the mixing in MIVMs, Reynolds number in MIVMs are defined as a linear combination of the stream velocities (or individual stream Re),[52]

$$Re = \sum_{i=1,4} \frac{D u_{jet,i}}{v_i}, \tag{8}$$

with $D$ the chamber diameter, $v_i$, and $u_{jet,i}$ the kinematic viscosity and the average velocity of inlet stream $i$. Liu et al. found that operation of MIVMs at Re above 1600 ensures good micromixing.[52]

Reynolds numbers for T-jet mixers are also sometimes defined differently. For instance, in some cases for T-mixers, the hydraulic diameter $2wd/(w + d)$ with $w$ being the chamber width has been used instead of the nozzle diameter $d$ in Equation (7).[66,106]

## 2.3 | Beyond IJMs: related mixing technologies

Beyond the conventional IJM designs, various other mixing apparatuses have been explored and documented in the literature, each with specific mixing performances, capacities, and applications in mind. In the context of this review, a brief overview of mixing technologies related to IJMs is given.

Like IJMs, static mixers are used to improve micromixing without any moving mechanical parts. Static mixers are a series of inserts or elements strategically arranged within equipment to accelerate mixing and increase energy dissipation rates.[107,108] For an overview related to static mixers, we refer to several reviews that have been published on this topic.[108–111] Static mixers outperform traditional mixing equipment but fall short of the superior performance delivered by IJM, see further in Table 2.

Lastly, miniaturized mixing equipment such as microfluidic mixers and microstructured mixer operated in the laminar regime have

**TABLE 2** Estimates for mean energy dissipation rates ($\bar{\varepsilon}$) as reported in the literature for different types of mixing equipment.

| Equipment | $\bar{\varepsilon}$ (W kg$^{-1}$) |
| --- | --- |
| Stirred tanks[108] | 10–100 |
| Static mixers[108,243] | 100–1000 |
| Rotor stator mixers[244] | 100–1000 |
| Submerged impinging jet mixers[30,105] | 1000–10,000 |
| Confined impinging jet mixers[29] | 10,000–100,000 |

*Note*: Typically $\varepsilon$ in the order of 10$^5$ W/kg leads to micromixing times of the order of 1 ms for low viscous liquids.[72,242]

become increasingly popular.[112–114] However, the micromixing process tends to be comparatively slower than that observed in IJMs due to the absence of turbulence. Micromixers are categorized into passive (solely relying on pumping energy) and active (utilizing external energy sources) mixing devices.[114] For discussions concerning the various micromixer types, extensive reviews on the subject are available.[110,112–114]

# 3 | MIXING CHARACTERIZATION

## 3.1 | Experimental approaches

As the name suggests, the primary role of IJMs is to facilitate fast mixing. Consequently, evaluating the performance of IJMs hinges on effectively characterizing the mixing required to achieve complete homogeneity. However, quantifying turbulence and mixing at microscales poses significant challenges due to the short time and small length scales at which the mixing process unfolds.

A distinction is made between experimental (e.g., References 8,11,23,27–29,36,37,80) and computational methods (e.g., References 26,33,50,51,54,115). For the experimental approaches, a second distinction is made between physical and chemical methods.[25] The analysis of characterization experiments can be challenging due to the absence of standardized quantification methods.[25] Moreover, methods have evolved over the years, progressively becoming more precise (e.g., compare References 8 and 36), adding an additional layer of complexity to results' interpretation.

### 3.1.1 | Physical methods

Physical methods employed for mixing characterization in IJMs primarily involve flow visualization experiments,[8,24,28,36,116] sometimes coupled with velocimetry measurements.[26,33,64,69,80,103] A second type of mixing characterization takes on a more pragmatic approach by evaluating whether the degree of mixing of an IJM is sufficient for the intended process by directly assessing the actual quality of the end product.

*Flow visualization*

Typically flow visualization experiments consist of mixing a transparent liquid with a colored (dyed) liquid.[25] This method of course implies that the IJM is optically accessible, which is not necessarily the case. Most important for visualization methods is that the resolution is sufficiently high to detect the smallest scales of segregation. If this is not the case, it is impossible to determine whether the two fluids are effectively mixed.[25]

By visualizing the spreading and mixing of the dye, different flow patterns can be identified, see Section 4.1. Mixing in IJMs above Re$_{crit}$ is inherently transient and characterized by short residence times.[26,37] As a result, such flow visualization experiments are generally time-dependent.

Some studies have used fluorescent dyes to increase the sensitivity of flow detection through the use of planar laser-induced fluorescence (PLIF).[8,26,27,51,85,117] In PLIF a fluorescent dye is excited by a laser and the emission of the dye is recorded. PLIF is useful to assess mixing in IJMs, as the temporal resolution is solely constrained by the pulse rate of the laser (typically in the ms range).[85]

More quantifiable mixing characterization using flow visualization can be done by tracking the color progression in a local zone.[25] The quality of mixing can then be defined using, for example, the intensity of segregation ($I_S$),[118] which can be considered as a measure for the state of subdivision of eddies. The $I_S$ can be calculated using

$$I_S = \frac{\sigma^2}{\sigma_{\max}^2} \text{ with } \sigma^2 = \frac{1}{V}\int_V (c-\bar{c})^2 dV, \qquad (9)$$

with $\bar{c}$ being the mean value of the concentration field, $c$ (mol/m$^3$) being the local concentration, and $\sigma_{\max}^2$ being the maximum variance.[118] The $I_S$ has been calculated in several IJM studies.[8,26,43,59] A low $I_S$, that is, good mixing, for one chemical species does not necessarily imply effective mixing with other chemical species in multicomponent mixtures.[82] In other cases, a mixing time is calculated, see Section 3, by determining the time required to reach a specific mixing criterion.[25]

Dye spreading analysis must always be interpreted with care, as such measurements rely on perpendicular imaging which may lead to misinterpretation of the results.[25] With sufficiently high spatial resolution, the lamellar flow structure may become visible in downstream regions from the impingement point, enabling the direct extraction of an estimate of the striation thickness from visualization experiments.[8,28] Another consideration to take into account is the diffusion rate of the utilized dye, which might vary from that of the process streams, potentially leading to erroneous mixing times.[109]

Flow visualization in IJMs has also been coupled with classical velocimetry methods. For instance, laser doppler anemometry (LDA) has been used,[65,80,81,103] which measures the Doppler shift in a laser beam to measure the fluid velocity field in the IJM. LDA offers precise point-wise velocity measurements but lacks a comprehensive view of the instantaneous flow field due to its inherently localized measurements.[64]

In contrast, particle image velocimetry (PIV) has been employed for characterizing mixing in IJMs, leveraging the advantage of capturing
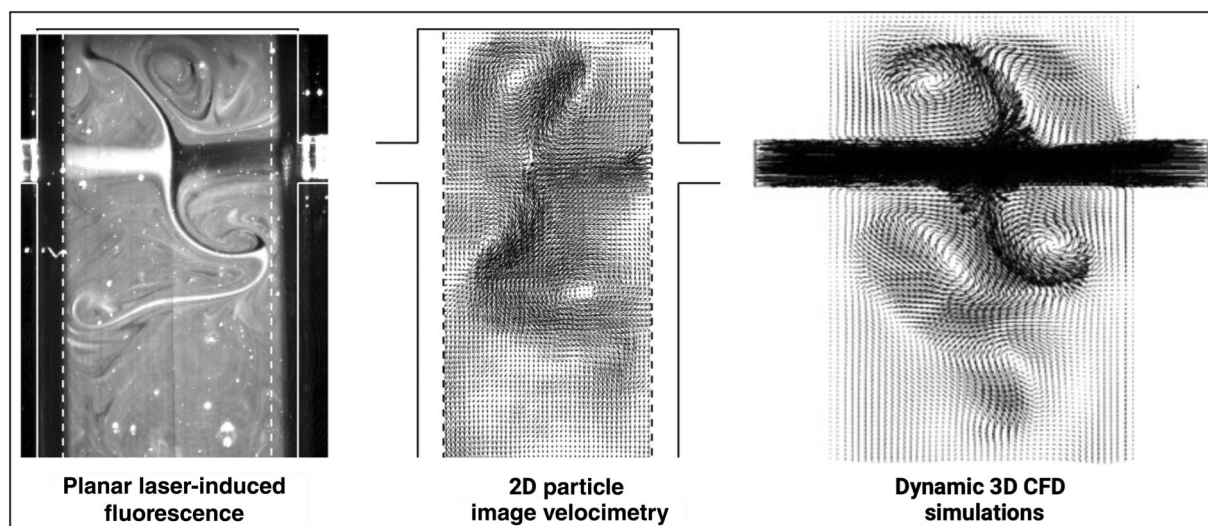
**FIGURE 6** Flow visualization to characterize mixing in a confined impinging jet mixer (CIJ) ($d = 1.5$ mm, $D = 10.0$ mm, $h = 5.0$ mm, $H = 50.0$ mm) at the impingement point for Re = 200 using PLIF (left), PIV (center), and 3D CFD simulations (right).[65] Adapted from Santos et al. .[65] Created with BioRender.com. Copyright ©2009 American Institute of Chemical Engineers (AIChE).

larger-scale flow patterns simultaneously.[26,33,51,64,69,79,84,119] In PIV, images captured at known time intervals apart, depicting seeded particles moving within the IJM illuminated with a sheet of light, are cross-correlated by region to precisely determine the instantaneous particle velocities. PIV results in two-dimensional slices showing the particle flow fields. One of the main advantages of PIV compared to PLIF is that it gives a value for the vorticity.[51] Figure 6 provides a comparison between flow visualization techniques using PLIF and PIV, alongside CFD simulations,[65] discussed in Section 3.2.

### Product-based evaluation

By evaluating the product of the mixing process, the mixing performance can be evaluated in terms of the intended and desired application. In the past, the quality of mixing was sometimes judged merely by the visual appearance of the product.[28] Tucker and Suh[36] suggested a more quantifiable approach by measuring the variance of the concentration of one component from a number of small samples. In such an experiment, smaller variances imply better mixing.[36] The variance can then also be related to the segregation scale.[36] Another method involved measuring heat release during exothermic mixing-dependent processes, such as during urethane polymerization.[28,38,43] While these examples provide a glimpse into diverse evaluation methods, it is important to recognize that this is not an exhaustive summary, and additional methods exist.[103]

### 3.1.2 | Chemical Methods: Test Reactions

One of the most common and effective methods to characterize micromixing in IJMs is with test reactions, also called reactive tracer tests.[6,70,120,121] This approach is grounded in the notion that a

chemical reaction can transpire only when reagents are adequately mixed at the microscale.[6] When competitive reactions occur with an intrinsic reaction time in the same order of magnitude as the mixing time (i.e., in the mixing-sensitive regime), mixing dictates the timescale of the reaction progression.[6] Fast microscale mixing favors the fastest reaction, while slow mixing results in more reagents being consumed by the slower reaction.[6]

### Methodology

Chemical probe methods rely on the competition between two reactions for a common reagent in stoichiometric deficit.[122] Both competitive-consecutive and competitive-parallel reactions have been used.[6,25,123,124] These reactions, shown schematically as simplified reaction schemes in

$$
\begin{aligned}
&\textbf{Competitive} - \textbf{consecutive} \\
&\quad A + B \xrightarrow{\ k_1\ } R \\
&\quad B + R \xrightarrow{\ k_2\ } S \\
&\textbf{Competitive} - \textbf{parallel} \\
&\quad A + B \xrightarrow{\ k_1\ } R \\
&\quad B + C \xrightarrow{\ k_2\ } S,
\end{aligned}
\tag{10}
$$
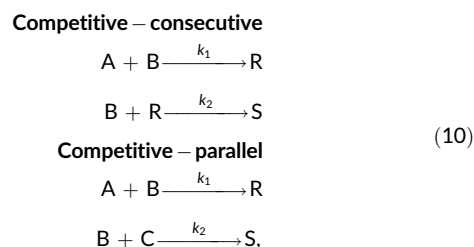
must have well-defined kinetics.[6] Specifically, the first reaction should exhibit quasi-instantaneous kinetics, while the second reaction should be rapid ($k_1 \gg k_2$), characterized by a time scale comparable to the mixing time (i.e., for optimal sensitivity, $\tau_{\text{mixing}} \approx \tau_{\text{reaction}}$).[6]

The formation of product $S$ is then related to Da, see Figure 7, and is considered as an indicator of the mixing quality.[25] The experimentally recorded amount of product can then be used to calculate a segregation index ($X$),
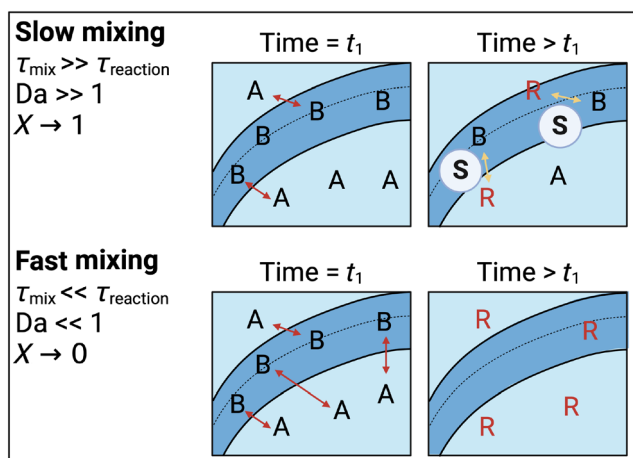
**FIGURE 7** Schematic overview of the effect of fast and slow micromixing (with respect to the reaction rate) within a lamellar microstructure (see Figure 4) on the product distribution during a competitive reaction as shown in Equation (10). Adapted from Johnson and Prud'homme.[29] Created with BioRender.com. Copyright ©2003 American Institute of Chemical Engineers (AIChE).

$$X = \frac{2C_S}{2C_S + C_R}. \tag{11}$$

Fast micromixing corresponds to a low $X$ value, which approaches 0 for perfect mixing conditions. Slow mixing leads to higher $X$, which approaches 1 for total segregation.

The value of the segregation index $X$ is strongly dependent on the protocol conditions and thus only provides preliminary mixing information.[25,122] For instance, for IJMs, depending on the flow ratios of the two streams, the concentrations of the inlet streams in the protocol of choice need to be changed. Falk and Commenge[25] advise adjusting the ratio of the molar flow rates of the reactants in the two inlet feeds to match molar number ratios from optimized batch protocols.

To obtain an absolute parameter for mixing characterization, the mixing time ($\tau_{\text{mixing}}$) must be calculated from the segregation index and a specific mixing model.[6,122] Chemical tracer tests inherently lack spatially-resolved mixing information, thus providing only global mixing insights, but this limitation is not necessarily problematic within IJM mixing characterization.[125]

Two widely adopted reaction systems for assessing micromixing are the competitive-consecutive reactions involving 1-naphthol[120] and 2-naphthol,[126] collectively known as the Bourne reactions, developed during the 1980s and 1990s. Another extensively utilized system is the iodide-iodate reaction, referred to as the Villermaux-Dushman reaction, established in the 1990s.[123,124] Both reaction systems offer the advantage of product quantification through spectrophotometric measurements.[120,123,124,126]

*Use in IJMs*

Several authors have used these tests to characterize micromixing in IJMs. In 1987, Kusch et al. [37] investigated micromixing in an IJM

($d = 1.02$ mm, $D = 5.00$ mm) across Re values from 50 to 500, employing the azo dye coupling reaction with 1-naphthol and diazotized sulfanilic acid.[37] Their data exhibited a lot of scatter, which could be due to time-varying mixing patterns,[37] but is more likely a result of variations in the momentum ratio,[24] see Section 5. The characteristic reaction time recorded for their experiments was 3–12 s,[37] which is several orders of magnitude longer than later and more accurate experiments in comparable IJMs suggest.[29]

Mahajan and Kirwan[23] also employed the Bourne reaction scheme, opting to elevate both temperature and reactant concentrations to their maximum values before decomposition to enhance sensitivity. They achieved a rapid characteristic reaction time of only 65 ms in a nonsubmerged IJM ($d = 0.5$ mm, $D = 2.54$ mm) at Re = 1200.[23]

Johnson and Prud'homme[29] used the fast sodium hydroxide with hydrogen chloride neutralization and the slower acid-catalyzed hydrolysis of 2,2-di-methoxypropane to acetone and methanol (as proposed by Baldyga et al. [75]) scheme in a CIJ (e.g., $d = 0.5$ mm, $D = 2.38$ mm). Reaction times as low as 9.5 ms were recorded for Re values ranging from 100 to 3000.[29] The same reaction system was used by Gillian and Kirwan[46] in a CIJ ($d = 0.50$ mm, $D = 2.38$ mm) and T-jet mixers ($\theta = 0$–$10°$, $d = 1.30$ mm), who found mixing times of the order of 10 ms. These values match well with mixing times calculated from volume-averaged mixing times extracted from CFD simulations,[53,56,58] see Section 3.2.1. For instance, Marchisio et al. [58] found mixing times ranging from 50 to 2 ms (for $d = 1$ mm, $D = 4.8$ mm, $H = 9.6$ mm) and from 100 to 5 ms (for $d = 2$ mm, $D = 9.96$ mm, $H = 19.2$ mm) for Re ranging from 200 to 2000.

Schaer et al. [30] used the Villermaux-Dushmann protocol[113,121] to evaluate micromixing times for an IJM ($d = 1$ mm, $D_{ns} = 10$ mm) immersed in a stirred tank reactor. At jet velocities exceeding 3 m/s, the impeller speed showed minimal influence, leaving micromixing entirely under the control of the impinging jets, resulting in reaction times as short as 4 ms.[30] Experimental mixing characterization studies in which viscosity is modified do so by adjusting the temperature or through the addition of viscosity-modifying additives (e.g., polyethylene glycol is useful as it only affects the viscosity and not the mass diffusivity[29,46]).[43]

In summary, chemical tracer tests have become standard practice to evaluate micromixing and have been used for characterizing various IJM configurations and experimental conditions.[24,127,128]

## 3.2 | Computational approaches

### 3.2.1 | Computational models

The starting point for almost all computational models for IJMs are based on the Navier-Stokes equations for mass and momentum balance of the fluid. Since this review focuses on mixing in the liquid phase, Navier-Stokes equations for incompressible flows should be used,

$$\nabla \cdot \boldsymbol{u} = 0, \tag{12}$$

$$\frac{\partial \boldsymbol{u}}{\partial t} + \boldsymbol{u} \cdot \nabla \boldsymbol{u} = -\frac{1}{\rho}\nabla p + \nabla \cdot (\nu \nabla \boldsymbol{u}), \quad (13)$$

with $\boldsymbol{u}$, $p$, $\rho$, and $\nu$ representing the velocity, pressure, density, and kinematic viscosity of the fluid, respectively.

Direct numerical simulation (DNS) of Equations (12) and (13) provides accurate information about the flow and pressure field inside the IJM, as verified in Reference 129 through comparison with experimental PIV results. In addition to flow and pressure distributions, detailed DNS results also aid in understanding turbulent kinetic energy distribution within the IJM, revealing regions of heightened turbulent dissipation and, consequently, more efficient mixing.[82] While DNS is accurate, it requires spatial resolution of the Kolmogorov length scale ($\lambda$) to capture turbulent effects. This makes the method computationally expensive, especially at large Re; thus turbulence models based on Reynolds-Averaged Navier Stokes (RANS) or Large Eddy Simulation (LES) are frequently used to model turbulence in IJMs. Nevertheless, DNS results continue to be useful to benchmark turbulence models for IJMs.[49,54] In References 82 and 115, Equations (12) and (13) were extended to account for the distribution of nonreacting passive scalars, such as concentrations of constituent liquids and chemical components in the IJM. By representing the concentration of the $i$th scalar as $\xi_i$,

$$\frac{\partial \xi_i}{\partial t} + \boldsymbol{u} \cdot \nabla \xi_i = \frac{1}{\mathrm{Re} \cdot \mathrm{Sc}}\nabla^2 \xi_i, \quad (14)$$

is obtained.

DNS of Equations (12)–(14) revealed that $\xi_i$ is rapidly diffused as the shear layer, see Section 4.1, breaks down into small-scale vortices. However, accurate computation of $\xi_i$'s requires the spatial resolution of the Batchelor length scale, which is related to the Kolmogorov length scale as $\lambda_B = \lambda/\sqrt{\mathrm{Sc}}$. This makes DNS computationally expensive and less prevalent, especially for large Sc. A more common approach to understand distribution of scalars involves using one-point probability distribution functions (PDFs) of the composition of the mixture,[130,131] whose transport is governed by

$$\frac{\partial f_\xi}{\partial t} + \nabla \cdot (\langle \boldsymbol{u}|\boldsymbol{\psi}\rangle f_\xi) + \frac{\partial}{\partial \psi_i}\left[\langle \nabla \cdot (D_{\xi_i} \nabla \xi_i)|\boldsymbol{\psi}\rangle f_\xi\right] + \frac{\partial}{\partial \psi_i}(S_i f_\xi) = \boldsymbol{0}, \quad (15)$$

where $f_\xi(\boldsymbol{\psi}; \boldsymbol{x}, t)$ is the composition PDF, $\boldsymbol{\psi}$ is the composition space vector, $D_{\xi_i}$ is the molecular diffusivity, and $S_i$ is the reaction rate of species $i$. The second and the third terms in Equation (15), which, respectively, represent transport in physical space due to velocity (advection) and transport in composition space due to mixing (diffusion) of $f_\xi$, contain conditional probability expressions which need to be modeled.[71,132] For modeling, an estimate of the mean flow is necessary, for which RANS and LES are commonly used.

In RANS models, the velocity field is decomposed into a time–averaged mean component and a fluctuating component, whose mean value is 0, like $\boldsymbol{u} = \langle \boldsymbol{u}\rangle + \boldsymbol{u}'$. Substituting this into Equations (12) and (13), no additional terms are introduced in Equation (12). However, in

an additional term appears in the momentum balance in the right-hand side,

$$\frac{\partial \langle \boldsymbol{u}\rangle}{\partial t} + \langle \boldsymbol{u}\rangle \cdot \nabla \langle \boldsymbol{u}\rangle + \frac{1}{\rho}\nabla \langle p\rangle - \nabla \cdot (\nu \nabla \langle \boldsymbol{u}\rangle) = -\frac{1}{\rho}\nabla \cdot (\rho \langle \boldsymbol{u}'\boldsymbol{u}'\rangle) = -\frac{1}{\rho}\nabla \cdot \boldsymbol{\tau}', \quad (16)$$

which is referred to as the divergence of Reynolds stress. Different closure models have been proposed for the Reynolds stress ($\boldsymbol{\tau}'$), which can be broadly classified into linear eddy-viscosity (LEV), nonlinear eddy–viscosity (NLEV) and explicit algebraic Reynolds–Stress (EARS) models; all of which have been extensively reviewed in the literature.[71,133] Typically, LEV and EARS models are used for isothermal applications, whereas NLEV models are more common when temperature variations inside the IJM are significant.[129] All of these models require the solution of an equation that governs the transport of turbulent kinetic energy ($k$); and an additional equation which governs the length scale of turbulence (both $\epsilon$ and $\omega$ are commonly used).[133] For the specific case of isothermal mixing in CIJs; the Speziale, Sarkar and Gatski,[134] Launder, Reece and Rodi (LRR)[135] and Shear Stress Transport $k\text{-}\omega$[136] models were compared in Reference 137, where LRR model results provided the best fit to experimental observations from Reference 49. However, choosing appropriate RANS models for IJMs still continues to be an area of active investigation.

In LES models, a spatial filter such as $G(\boldsymbol{r}, \boldsymbol{x})$ is used to define a filtered velocity $\overline{\boldsymbol{u}}$,[71] $\overline{\boldsymbol{u}} = \int_{-\infty}^{\infty} G(\boldsymbol{r}, \boldsymbol{x})\boldsymbol{u}(\boldsymbol{x} - \boldsymbol{r}, t)\mathrm{d}\boldsymbol{r}$. Spatially filtering Equations (12) and (13) does not result in additional terms in the mass balance, but pick an additional divergence of a subgrid-scale (SGS) stress term ($\tilde{\boldsymbol{\tau}}$) in the momentum equation, as shown in the right-hand side,

$$\frac{\partial \overline{\boldsymbol{u}}}{\partial t} + \overline{\boldsymbol{u}} \cdot \nabla \overline{\boldsymbol{u}} + \frac{1}{\rho}\nabla \overline{p} - \nabla \cdot (\nu \nabla \overline{\boldsymbol{u}}) = -\frac{1}{\rho}\nabla \cdot \tilde{\boldsymbol{\tau}}. \quad (17)$$

The term $\tilde{\boldsymbol{\tau}}$ is resolved using models such as the eddy-viscosity model,[138] where $\tilde{\boldsymbol{\tau}}$ is assumed proportional to the filtered rate of strain, that is, $\tilde{\boldsymbol{\tau}} = -\rho\nu_{\mathrm{SGS}}(\nabla \tilde{\boldsymbol{u}} + \nabla^{\mathsf{T}}\tilde{\boldsymbol{u}})$. The proportionality coefficient $\nu_{\mathrm{SGS}}$ is called the SGS viscosity and is defined as a function of the width of the filter.[139] More sophisticated models, which consider the decomposition of $\tilde{\boldsymbol{\tau}}$ into constituents such as Leonard stress and Clark stress using the Germano identity have also been proposed, for details see Reference 140. LES was first presented for turbulent reacting flows in Reference 141 and developed for IJMs in particular.[55] There has also been some work where RANS and LES models have been combined to resolve the flow inside IJMs.[26,142] Owing to the smaller computational cost of RANS as compared to LES models, they are more commonly employed today.

In the subsequent discussion in Section 3.2, we will use $\langle \boldsymbol{u}\rangle$ to represent the resolved part of the velocity and $\boldsymbol{u}'$ to represent the unresolved part for both LES and RANS.[†] Using this notation, Equation (15) can be rewritten as[143]

---

†We choose this notation as most of the simulations for IJMs use RANS models, where this representation is commonly employed. However, the underlying concepts for micromixing are the same for RANS and LES.

$$\frac{\partial f_\xi}{\partial t} + \langle \boldsymbol{u} \rangle \cdot \nabla f_\xi + \nabla \cdot (\langle \boldsymbol{u}' | \boldsymbol{\psi} \rangle f_\xi) + \frac{\partial}{\partial \psi_i}(D_{\xi_i} \nabla^2 \langle \xi_i \rangle f_\xi)$$
$$+ \frac{\partial}{\partial \psi_i} \left[ \langle \nabla \cdot (D_{\xi_i} \nabla \xi_i') | \boldsymbol{\psi} \rangle f_\xi \right] + \frac{\partial}{\partial \psi_i}(S_i f_\xi) = \boldsymbol{0}, \tag{18}$$

where the second term represents transport in physical due to mean velocity (macromixing), the third term represents transport in physical space due to scalar conditioned velocity variations (mesomixing), and the fourth and fifth terms represent the transport in composition space due to molecular mixing (micromixing).[137,143] Note that the fourth term, which represents molecular diffusion, is negligible at high Re and is usually ignored.[137] The mesomixing term is usually approximated using the gradient diffusion model $\langle \boldsymbol{u}' | \boldsymbol{\psi} \rangle f_\xi = -\Gamma_t \nabla f_\xi$,[144] where $\Gamma_t$ represents the turbulent diffusivity. The turbulent diffusivity is a function of the turbulent kinetic energy, turbulent dissipation and $Sc_t$ (turbulent Schmidt number).[132] Although originally proposed for isotropic flows, the gradient diffusion model is almost ubiquitous because of simplicity, satisfactory accuracy and computational ease. The micromixing term is commonly approximated using the interaction–by–exchange–with-the-mean (IEM) model,[145] which essentially models micromixing as a linear relaxation of the scalar concentrations toward their mean.[71,132] This approach has been used to quantify micromixing in IJMs in References 50,54,55, and 146, among others. However, the IEM model assumes that all the scalars in a mixture mix with a single characteristic time scale, which may be nonphysical for some mixtures where the Sc values are very dissimilar. An improvement to the IEM called the Fokker-Planck mixing model,[147] has been applied recently to model micromixing in a CIJ.[137]

After making these modeling assumptions, Equation (18) is solved for $f_\xi$. Solution methods include full simulations of Equation (18) using notional fluid particles in the Lagrangian frame of reference,[148,149] also referred to as transported PDF methods. However, this is computationally expensive and less pursued for IJMs.[132] The more widely used solution method for Equation (18) is the so-called presumed PDF method, where a form for the joint scalar PDF is assumed.[132] A common choice is that the PDF is composed of Dirac delta functions,[150] such that

$$f_{\xi,Y_2} = \sum_{n=1}^{N_e} p_n \prod_{\alpha=1}^{N_s} \delta[\psi_\alpha - \langle \xi_\alpha \rangle_n] \delta[y_2 - \langle Y_{2\alpha} \rangle_n], \tag{19}$$

is obtained, with $N_s$ and $N_e$ representing the number of scalars and number of environments into which the PDF is discretized, respectively, and $p_n$ represents the probability of environment $n$. The variable $Y_2$ represents the reaction progress variable, which becomes significant when the PDF describes the composition for a mixture where mixing and reaction times are comparable, that is, $Da \sim 1$. The number of environments has been varied between 2 and 5 in the literature,[151] and it was concluded that $N_e = 3$ provides the best trade-off between accuracy and computational cost. The concentrations of the various constituents in the mixture can be described as a function of $\langle \xi_\alpha \rangle$, $\langle Y_{2\alpha} \rangle$, and $p_n$ at any point inside the mixer.[132] Taking different moments of the presumed PDF, the mean and variance of $\xi_i$'s can be calculated, which are used to model micromixing in the

IJM. A combination of the assumed PDF method using Dirac delta functions with the IEM micromixing model, also referred to as DQMOMIEM[152] has been most commonly used to model mixing in IJMs, and obtain good agreement with experiments. Other presumed PDF models include beta PDF methods[153] and gamma PDF methods,[154] and fitting experimental data using other forms continues to be an active area of investigation. On a side note, since IJMs are frequently used for crystallization, the development of equations for turbulent mixing enumerated in this section have been closely coupled with transport equations for crystallized particles in the IJM in the literature.[132] Numerous detailed reviews on these transport equations, also referred to as population balance models (PBMs) have been published, for details see Reference 155.

### 3.2.2 | Analytical approaches

Also mathematical modeling has been employed to investigate jet impingement, for example, for the case of single free-surface jet impingement on a normal plane,[77,156–158] or for impinging jets colliding head-on.[159–161] By utilizing geometric symmetries, it is possible to derive an analytical solution for a partial differential equation that represents the local flow field close to the interface between two impinging jets. A mirror image model was introduced by Powell,[162] in which the impingement between two opposing jets at a distance is described, provided that the impingement plane and the impingement zone are symmetrical. Nosseir et al.[163] and Tamir[4] suggested that the mirror image notion might hold true for laminar flows in impinging jets but could be challenging to apply to turbulent flows. Powell's mirror image model aids in the understanding of some global parameters and their profiles in impinging streams, for example, the velocity field, but its main limitation is that it ignores the interaction between the opposing streams upon impingement. By employing separation of variables and eigenfunction expansion,[159,164,165] the solution can be derived under certain assumptions. Tamir[4] investigated the velocity field in laminar impinging streams using Powell's mirror image model and general fluid dynamics principles. Assumptions made for the analytical solution include the following: The fluid is incompressible, inviscid, and at steady state; the flow is assumed to be axisymmetric, with the two impinging jets having the same velocity field but opposing directions; the flow is irrotational; the influence of gravity is minimal. The concentration is uniform at the nozzle inlets and there is no mass flux at the interfaces (including very far from the centerline). The equations governing fluid motion can then be derived from

$$\rho \boldsymbol{u} \cdot \nabla \boldsymbol{u} = -\nabla p. \tag{20}$$

For planar two-dimensional impinging streams, $\boldsymbol{u} = u_x \boldsymbol{i} + u_y \boldsymbol{j}$,

$$u_x \frac{\partial u_x}{\partial x} + u_y \frac{\partial u_x}{\partial y} = -\frac{\partial p}{\partial x}, \quad u_x \frac{\partial u_y}{\partial x} + u_y \frac{\partial u_y}{\partial y} = -\frac{\partial p}{\partial y}. \tag{21}$$

is obtained.

Assuming an ideal fluid flow case where the flow is irrotational, the concept of a velocity potential is employed. In the Stream function-Potential ideal flow approach, irrotational flow is assumed. However, for the Vorticity-Stream function approach, irrotationality is not assumed by default. From irrotational flow and continuity,

$$\frac{\partial u_x}{\partial y} - \frac{\partial u_y}{\partial x} = 0, \quad \frac{\partial u_x}{\partial x} + \frac{\partial u_y}{\partial y} = 0. \tag{22}$$

is found. The velocity in terms of the stream function $\psi$ and the velocity potential $\phi$ relationships are

$$u_x = -\frac{\partial \psi}{\partial y} = -\frac{\partial \phi}{\partial y}, \quad u_y = \frac{\partial \psi}{\partial x} = -\frac{\partial \phi}{\partial x}. \tag{23}$$

For axial-symmetric impinging streams, it is more convenient to use cylindrical coordinates, leading to

$$u_r = \frac{1}{r}\frac{\partial \psi}{\partial z} = \frac{\partial \phi}{\partial r}, \quad u_z = \frac{1}{r}\frac{\partial \psi}{\partial r} = \frac{\partial \phi}{\partial z}, \quad u_\theta = 0. \tag{24}$$

### Stream-potential ($\psi$-$\varphi$) approach

Pressure and velocity are conveniently expressed in terms of the velocity potential ($\varphi$) and the stream function ($\psi$). It is more practical to use the cylindrical coordinates for the stream function when dealing with axially symmetric impinging streams. It is challenging to develop a stream function that satisfies the continuity equation for general three-dimensional impinging streams. Even though these findings do not fully capture the flow characteristics of impinging streams, the study by Wu[161] about pressure and velocity profiles aids in understanding the features and some regularity of impinging streams. A thorough examination of the impingement's boundary layer is necessary to calculate the mass transfer rates and wall shear stress accurately under an impinging jet.

The velocity potential can be represented as

$$\varphi(x,y) = -0.5M(-x^2 + y^2), \quad \varphi(r,z) = -0.5M(-2z^2 + r^2), \tag{25}$$

with $M$ being a constant (see Figure 8).

Considering $d\psi = u_x dx - u_y dy$, the expressions for the velocity components can be derived as

$$\begin{aligned} u_x &= -Mx, \ u_y = My, \ u_r = -Mr, \\ u_z &= -2Mz, \frac{dy}{dx} = -\frac{y}{x}, \ p = p_0 - 0.5\rho M^2(-x^2 + y^2). \end{aligned} \tag{26}$$

The streamlines in two-dimensional impinging streams are shown in Figure 8, the slope of which demonstrates the direction of flow and is equal to the local velocity vector,

$$\boldsymbol{u} = (u_x^2 + u_y^2)^{0.5} = M(x^2 + y^2)^{0.5}. \tag{27}$$

The velocity profile is flat for big $x$ or $y$, according to this relationship, but it is minimal at the centerline and grows as $x$ or $y$ increases when
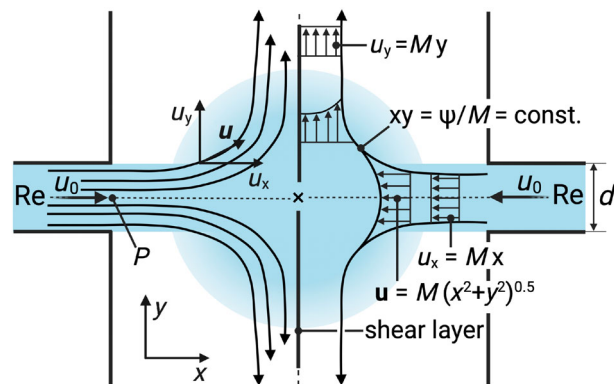


**FIGURE 8** Streamlines of two-dimensional impinging streams with velocity ($u_0$).[161] Streamline velocities and pressure distributions are indicated with $u$ and $P$, respectively. The impingement point is indicated with a cross. Recreated based on a figure from Wu.[161] Created with Biorender.com.

$x$ and $y$ are of the same order of magnitude (see Figure 8). As no shearing force is applied to the jets in the scenario when viscosity is neglected, these findings make sense. This results in the streamline equation: $xy = \psi/M =$ constant (see Figure 8).

**Stream-Vorticity ($\psi$–$\Omega$) Approach:** For two-dimensional and axisymmetric impingement flow with an arbitrary velocity profile, analytical solutions to the stream-vorticity equation are found in terms of a surface integral involving the vorticity function ($\Omega$). This enables an iterative determination of the stream function throughout the impingement region. Between the surface and the jet centerline, the stream function is zero. A solution was obtained by approximating the far-field and near-field expressions at designated points with the stream function expressions computed in terms of the vorticity function distribution. The governing equations and boundary conditions are

$$\begin{aligned} &\frac{\partial^2 \psi}{\partial y^2} + \frac{\partial^2 \psi}{\partial x^2} = \Omega = \frac{\partial u_x}{\partial y} - \frac{\partial u_y}{\partial x}, \\ &\psi(x,0) = 0, \ \psi(0,y) = 0, \\ &\frac{\partial \psi}{\partial x}(a,y) = 0, \ \psi(x,b) = F(x), \end{aligned} \tag{28}$$

$$\begin{aligned} &\frac{\partial^2 \psi}{\partial z^2} + \frac{\partial^2 \psi}{\partial r^2} - \frac{1}{r}\frac{\partial \psi}{\partial r} = r^2 \Omega = r\left(\frac{\partial u_r}{\partial z} - \frac{\partial u_z}{\partial r}\right), \\ &\psi(r,0) = 0, \ \psi(0,z) = 0, \ \frac{\partial \psi}{\partial x}(a,z) = 0, \ \psi(r,b) = F(r), \end{aligned} \tag{29}$$

for cartesian and cylindrical coordinates, respectively. The influx stream function, $F(x)$ or $F(r)$, can be determined from the given influx velocity profile at some distance, $b$, above the surface. The outflux streamlines are assumed to become parallel at some sufficiently large distance, $a$, from the jet centerline.

The general solution, in cartesian coordinates, subject to the boundary conditions is given by

$$\begin{aligned} \psi(x,y) &= \sum_{n=1}^{\infty}\left[A_n \sinh(\gamma_n y) - \sum_{m=1}^{\infty}\frac{B_{mn}}{\gamma_n^2 + \alpha_m^2}\sin(\alpha_m y)\right]\sin(\gamma_n x), \\ \Omega(x,y) &= \sum_{m=1}^{\infty}\sum_{n=1}^{\infty}B_{mn}\sin(\alpha_m y)\sin(\gamma_n x), \end{aligned} \tag{30}$$

and in cylindrical coordinates by

$$\psi(r,z) = \sum_{n=0}^{\infty} \left[ D_n \sinh(\lambda_n z) - \sum_{m=0}^{\infty} \frac{E_{mn}}{\alpha_m^2 + \lambda_n^2} \sin(\alpha_m z) \right] r J_1(\lambda_n r),$$

$$\Omega(r,z) = r^{-2} \sum_{m=1}^{\infty} \sum_{n=1}^{\infty} E_{mn} r J_1(\lambda_n r) \sin(\alpha_m z),$$

(31)

where

$$\gamma_n = [(2n-1)/2a]\pi, \quad \alpha_m = m\pi/b,$$

$$A_n = \frac{2}{a \sinh(\gamma_n b)} \int_0^a F(x') \sin(\gamma_n x') dx', \quad C_{mn} = \frac{-B_{mn}}{\gamma_n^2 + \alpha_m^2},$$

$$E_{mn} = \frac{4}{ba^2 J_1^2(\lambda_n a)} \int_0^a \int_0^b r'^2 \varphi(r',z') J_1(\lambda_n r') \sin(\alpha_m y') dz' dr',$$

$$D_n = \frac{2}{a^2 J_1^2(\lambda_n a) \sinh(\lambda_n b)} \int_0^a F(r') J_1(\lambda_n r') dr',$$

$$\sum_{n=1}^{\infty} A_n \sin(\gamma_n x) \sinh(\gamma_n b) = F(x),$$

$$B_{mn} = \frac{4}{ab} \int_0^a \int_0^b \varphi(x',y') \sin(\alpha_m y') \sin(\gamma_n x') dy' dx',$$

and $\lambda_n$ are roots of $J_0(\lambda_n a) = 0$. The simple inviscid corner flow solution, $\psi \approx xy$ can be recovered as $x$ and $y$ become very small.

The governing equations of mass transfer with their boundary conditions are

$$u_r \frac{\partial c}{\partial r} + u_z \frac{\partial c}{\partial z} = D \left[ \frac{1}{r} \frac{\partial}{\partial r} \left( r \frac{\partial c}{\partial r} \right) + \frac{\partial^2 c}{\partial z^2} \right],$$

$$\frac{\partial c}{\partial r}(0,z) = 0, \quad c(r,\infty) = c_1, \quad c(r,-\infty) = c_2.$$

(32)

Considering that the concentration gradient along the impingement plane ($\frac{\partial c}{\partial r}$) is negligible compared to along the centerline ($\frac{\partial c}{\partial z}$), using the scaling analysis where the simplified concentration equation has a unique analytical solution,

$$\frac{c - c_2}{c_1 - c_2} = \frac{1}{2} \left( \text{erf} \left( \frac{z}{z_{refm}} \right) + 1 \right),$$

(33)

with $z_{refm} = (D z_0 / u_{z_0})^{1/2}$.

# 4 | MIXING BEHAVIOR

## 4.1 | Flow regimes

Numerous studies have reported the existence of at least two distinct and discernible flow regimes separated by a breakage point (at $Re_{crit}$,

see Section 2): a segregated steady-state flow regime with poor mixing (Re < 90–100) and a dynamic chaotic flow regime with good mixing (Re > 100–120).[8,24,28,37,63,84] Figure 9 shows typical flow patterns observed in a CIJ (d = 1.50 mm, D = 10.00 mm, H = 50.00 mm) for different Re values.[8]

In contrast, the self-sustained chaotic flow regime refers to cases in which both streams are engulfed as a result of vortices being formed downstream of the impingement point in the impingement mixing zone,[64,80,82] see Figure 5.[8] Upon impingement of the two jets a nonrigid vortex core, also described as a thin pancake-like[80,84] (i.e., disk-shaped) core, and a shear layer are formed from which vortices are continuously released.[64,80,82] The ensuing vortex street consists of mixing zones in a highly dynamic time-dependent oscillatory state in which vortices are continuously engulfed and detached. This stretching and folding of fluid layers results in a large interfacial contact area between the two fluids. Continuing downstream from the impingement mixing zone and progressing into the parallel flow zone,[8,36] as depicted in Figure 5B for CIJs, the flow reorganizes, turbulent motions diminish, leading to a gradual transition into regular (laminar, thus parabolic) pipe flow.[26,36,166] In a CIJ, the impingement mixing zone typically extends over a length of 2D to 3D from the top, with the remainder of the chamber length constituting the parallel flow zone.[8] Generally, the chaotic flow regime, and particularly the impingement mixing zone, is characterized by significantly faster mixing compared to the segregated flow regime.

Further increasing Re, results in the pseudo-random oscillatory flow instabilities becoming increasingly pronounced.[8] This heightened instability leads to vortex formation, engulfment, and detachment progressively closer to the impingement zone,[8] causing a further reduction in the size of lamellar fluid structures,[8] that is, better mixing. Beyond a certain threshold Re, a plateau is occasionally observed, potentially due to limitations in the sensitivity of the characterization methods employed.[29] As Re continues to increase, the mixing will continue to improve asymptotically toward perfect mixing.

In CIJs, chamber walls affect the vortex dynamics,[29] for example, by inducing increased vortex shedding or by pushing vortices back towards the impingement point.[82] These phenomena induce flow instabilities, see Section 4.2, that improve mixing.[82] In contrast, in free IJMs the walls have little to no impact on the mixing process and thus do not affect the vortices ensuing from the impingement point. In submerged IJMs, besides the mixing of the two jets, also the interaction between the jet and the surrounding fluid is important.[117] Prior to impingement, the jets entrain surrounding fluid.[117] When the inter-nozzle separation is small ($D_{ns}/d < 5$), the surrounding fluid is estimated to make up 20 % of the mixing volume.[117]

As mentioned earlier, the mixing behavior in T-mixers is significantly different from that in CIJs. While a thorough exploration of flow regimes in T-jet mixers is beyond the scope of this work, it is noteworthy that, unlike CIJs, which commonly exhibit two distinct flow regimes, T-jet mixers display three to four regimes: stratified, vortex, engulfment, and chaotic flow,[106,167] depending on Re and the dimensions of the T-mixer.[167–170] Due to the (typically square) nozzles extending fully through the confinement chamber in T-jet
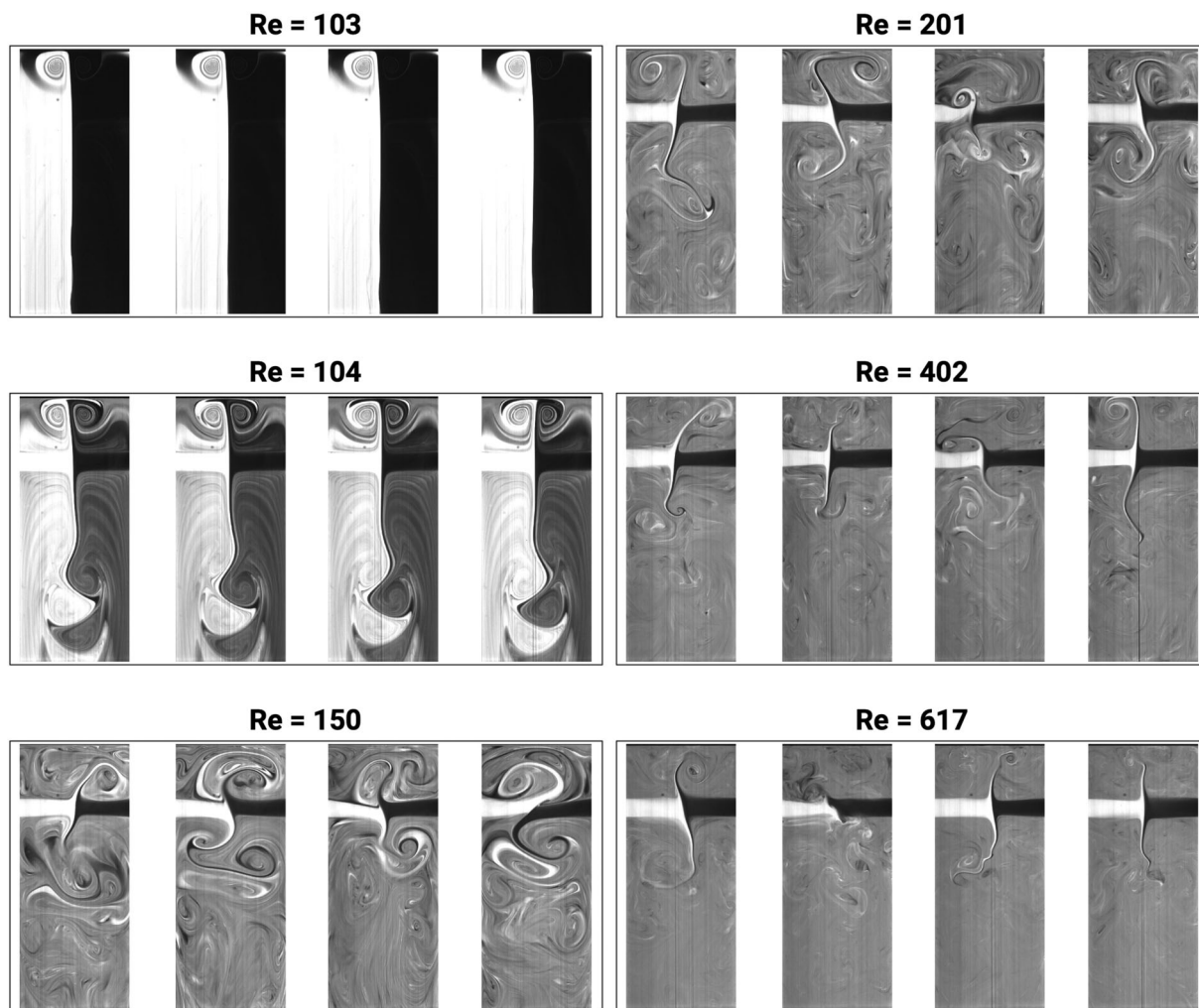
**FIGURE 9** Visualization (via planar laser-induced fluorescence) of flow patterns generated in the impingement mixing zone by mixing a nondyed with a fluorescent dyed liquid (with equal momentum) within a confined impinging jet mixer (CIJ) ($D/d = 6.66$, $D = 10$ mm) across various Re. The zone from the top of the cylindrical mixing chamber until 2.5$D$ is depicted. $Re_{crit}$ occurs at 111, but the dynamic oscillations start at Re > 120,[8] as identified by the characteristic periodic switching flapping motion.[8,116] A distinctive lamellar structure was detected at a distance of 2.5$D$ from the injectors, with the smallest striations measuring 15 $\mu$m in thickness. For Re > 600, no further reduction in $s$ could be detected. Adapted from Fonte et al.[8] Reprinted from Fonte et al., "Flow imbalance and Reynolds number impact on mixing in Confined Impinging Jets," Chemical Engineering Journal, Coypright (2015), with permission from Elsevier.

mixers,[2,171] there is no chamber for turbulence to develop, and the characteristic vortex core observed at the impingement point in CIJs[82] is absent in all T-jet mixer flow regimes.[2] Instead, upon impingement, the two fluid streams are immediately direct downwards and most mixing proceeds primarily downstream of the impingement point.[170] Further downstream, the flow approaches fully developed pipe flow and turbulence evolves from the walls toward the central axis,[170] as demonstrated in simulations and experiments by Bothe et al.[172]

## 4.2 | Dynamic behavior: self-sustaining oscillations

The distinctive dynamic behavior closely associated with the chaotic flow regime typically becomes noticeable when Re > 120,[8,65,68] see Figure 9. The vortex dynamics of impinging jets have been described

in numerous publications,[48,65,80–82,95,103,116,173–176] and play an important role in the mixing performance of CIJs.[65]

Three types of chaotic oscillations have been identified: At 150 < Re < 300, (i) radial deflective oscillations, causing periodic S-shaped flapping, occur,[84] see Figure 9. Above Re > 300, (ii) axial oscillations around the impingement point that emerge alongside radial deflective oscillations start to appear.[84] Beyond Re > 500, (iii) oscillations occur that lead to the decay or even disappearance of the shear layer near the impingement point.[84]

The origin and sustenance of these feedback-free oscillations remain debated, but typical features[82] have been identified.[‡] The collision of two axial jets results in the formation of a vortex core,[82,84,175] see Figure 10A–D. At the interface between the two

---

[‡]Many of these features are also relevant to IJMs with gaseous inlet streams, leading to cross-references in related research (e.g.,[84,177–179]).
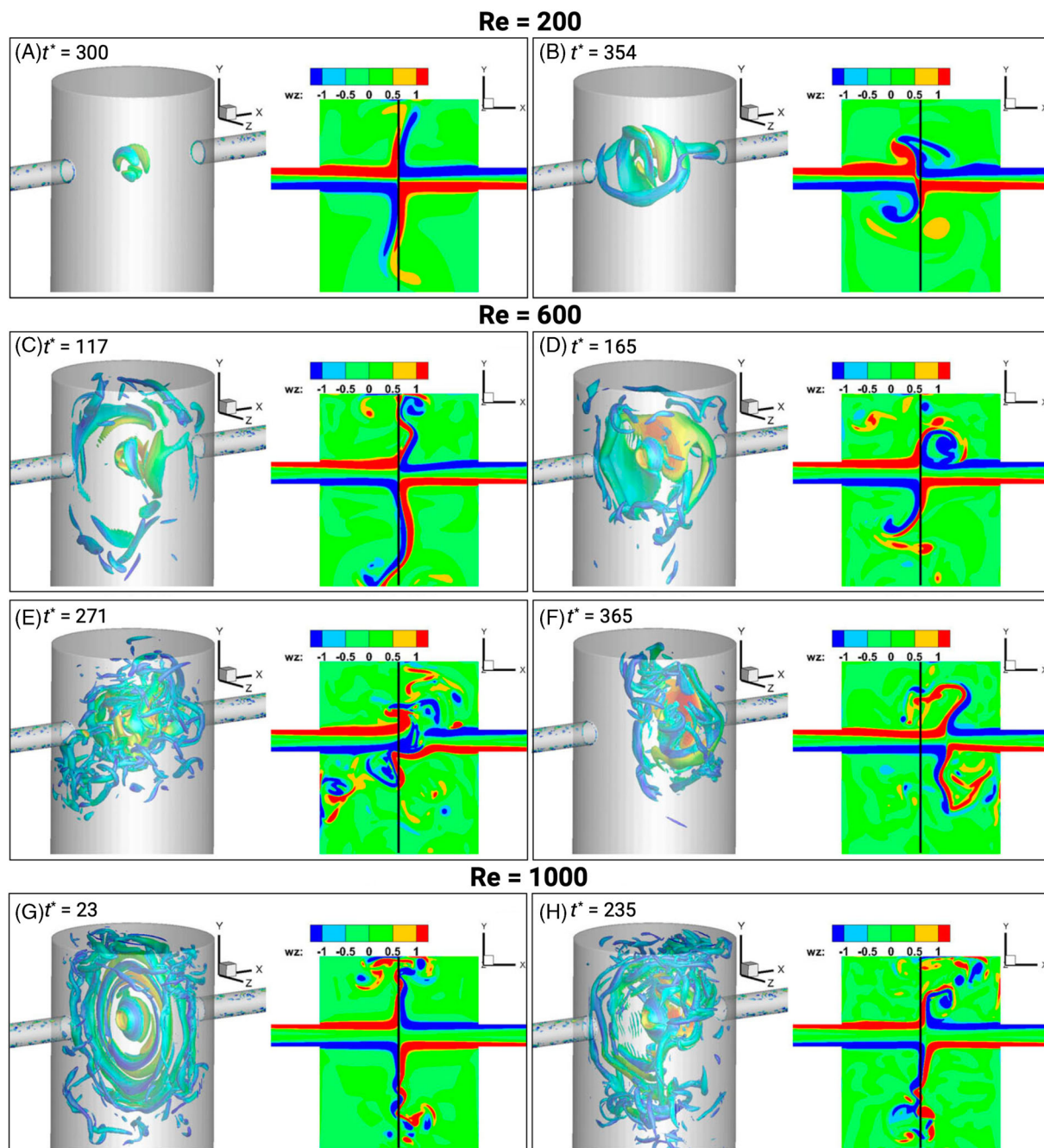
**FIGURE 10** The time evolution of the vortex dynamics (expressed in the characteristic time, $t^* = d/u_{jet}$) in the chaotic regime in three-dimensional and two-dimensional views (in the $z = 0$ plane) for Re = 200 (A, B), Re = 600 (C–F), Re = 1000 (G, H) in a confined impinging jet mixer (CIJ) ($D/d = 6.6$, $H = 12d$). Upon head-on impingement a pancake core is formed at the center of the shear layer, which continues to radially expand and shed vortices that reciprocally interact with the shear layer. Adapted from Hao et al. .[82] Original Figures by Hao et al. ,[82] Copyright 2020, licensed under Creative Commons CC BY.

streams there is a sharp velocity gradient, leading to the formation of a shear layer.[80,82,175] Radial deflective oscillations induce dynamic flapping of the shear layer[84] leading to the formation of vortices that radially roll up and are subsequently shed,[82] see Figure 10. Two mechanisms have been posited to explain these natural radial instabilities: They could result from (i) pressure disturbances induced by impingement of the opposing jets.[84] Such natural instabilities from impingement alone cannot fully explain the chaotic behavior in CIJs though.[48] Alternatively, (ii) the instabilities could be convective helical

instabilities occurring in free-flowing round jets at Re < 500.[84,180] The self-sustaining nature of these oscillations, as seen in CIJs, arises from their amplification under confinement: some of the shedded vortices in a CIJ reach the chamber walls and reciprocally return to the shear layer or even the inlet jet streams,[82] see Figure 10. This interaction with the walls and jets instigates a feedback loop of perturbations that destabilize the shear layer.[82,176] At higher Re (i.e., above 300), axial fluctuations in the jets (possibly due to axisymmetric instabilities in the inlet flows as observed in free-flowing jets at higher Re) induces

axial oscillations.[180] Icardi et al. have shown that small oscillations in the inlet flow indeed introduce additional chaos.[48,84] As Re increases even further (i.e., higher than 500), also downstream vortex structures become more interconnected leading to increased interactions among them,[65] eventually resulting in the oscillations that lead to the disruption of the shear layer itself.

Instabilities in the shear layer can cause the impingement point to shift away from the center axis, leading to increased asymmetric behavior,[82] or in some cases the auto-induced instabilities can grow so large that the jets miss each other completely.[80]

Spectral analysis of the dynamic flow field within CIJs suggests that there are typical oscillation frequencies[65,80,84,103,175] that can be related to eddy formation (i.e., the vortex shedding frequency, $\phi$, Hz = s$^{-1}$).[65] These typical frequencies can be identified as peaks in the power-frequency spectrum through a spectral analysis,[65,103] as illustrated in Figure 11. The power spectrum itself is obtained by squaring the magnitude of the Fourier transform applied to a time series of velocity data (extracted from LDA measurements or from numerical simulations).[48,65,81] Power spectra usually exhibit a large spread in frequencies, particularly at high Re,[48,65,81] underscoring the chaotic nature of the flow.[65] For instance in the results of Santos et al.[65] at Re = 600 the typical oscillation frequency is less well-defined than for Re = 250 due to the increased turbulence. Overall, a decrease in peak height of the typical frequency in the power spectrum at higher Re can be interpreted as a more turbulent and complex flow regime, characterized by the faster breakdown of vortices.[80,81,103]

The Strouhal number (St),

$$St = \frac{\phi d}{u_{jet}}, \tag{34}$$

is used to relate the jet velocity and the typical oscillation frequency ($\phi$) associated with vortex shedding, and can be considered as a dimensionless frequency.[103] If the fluctuations are too large to discern typical frequencies, such as those induced by modulated jet velocities,[96] the fluctuation frequency corresponding to the peak turbulent energy dissipation at different locations can be used as a representative St value.[96]

As Re increases from 100 to 250, the associated Strouhal number typically exhibits a steady rise from 0.01 to 0.1. Beyond this point, with further increases in Re, St values stabilize, and in some cases, may even exhibit a slight decrease (e.g., see the caption of Figure 11).[65,66,80,84,175] This suggests that, once a certain threshold for Re is surpassed, additional increases do not lead to enhanced oscillatory behavior and that the flow structures remain the same (as $\phi$ = constant). Moving from the jets' impact point to 30 mm further downstream, a decrease in St has been detected from 0.1 to 0.03.[65,175] Analogous analyses conducted in T-jet reactors exhibit comparable qualitative trends but different quantitative results, attributable to the difference in flow regimes and geometry.[181]

In addition to spectral analysis, a proper orthogonal decomposition can be applied to the flow field to give a spatial description of different flow structures and to separate them into orthogonal modes, which allows for identification of the main characteristics.[86]

Three-dimensional turbulence, see Section 1, involves an energy cascade from large to small eddies, culminating in heat dissipation via viscous dissipation, see Figure 7.[6] However, certain flows are better described by two-dimensional turbulence, where fluid motion in two planes follows an inverse-energy cascade from smaller to larger scales through eddy cannibalization.[182,183] Energy dissipation then primarily occurs through viscous stresses around evolving vortices.[68] Flow in CIJs exhibits characteristics of two-dimensional turbulence due to wall constraints.[68,95] Gonçalves et al.[95] demonstrated in their analysis of a CIJ's turbulence power spectrum ($d$ = 1.50 mm, $D$ = 10 mm, Re ranging from 200 to 500 in the 2D-case) that energy injection primarily occurs at the nozzle scale, subsequently transitioning into eddies resembling the chamber diameter ($D$).[95]
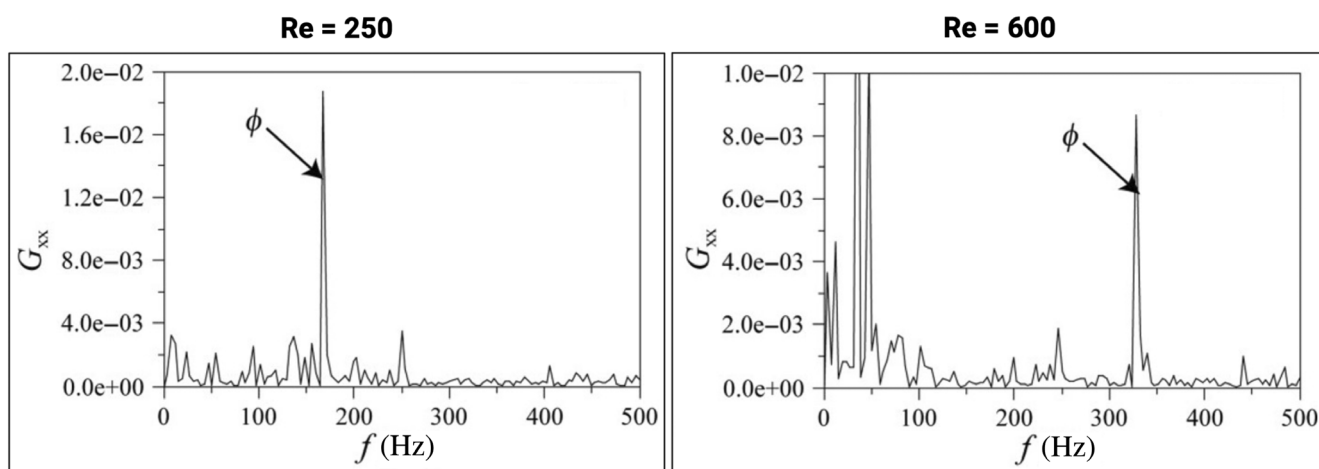


**FIGURE 11** Normalized power spectra of the velocity component along the jet axis, measured 5.0 mm below the impingement point for = 250 and Re = 600 in a confined impinging jet mixer (CIJ) ($d$ = 1.50 mm, $D$ = 10.00 mm, $H$ = 50.00 mm). laser doppler anemometry (LDA) and computational fluid dynamics (CFD) simulations within the same CIJ are shown in Figure 6. Typical frequencies ($\phi$) are indicated. At Re = 250, St = 0.066 ± 0.0075, and at Re = 600, St = 0.048 ± 0.0079. Adapted from Santos et al.[65] Copyright ©2009 American Institute of Chemical Engineers (AIChE).

## 4.3 | Energy dissipation analysis

Numerous studies discussed mixing in IJMs in terms of energy dissipation rates.[30,50,62,82,95,101,128,172,184,185] Mean energy dissipation rates ($\bar{\varepsilon}$) can be calculated using[29]

$$\bar{\varepsilon} = \frac{P}{\rho V_m}, \tag{35}$$

with $V_m$ being the mesomixing (i.e., the dissipation) volume and $P$ being the power, from macroscopic mass and (mechanical) energy balances over the impingement zone,[29,46,128] for instance, by assuming completely inelastic jet collision and outlet kinetic energy of zero.[23,128] Depending on the chosen characteristic dimension ($D$ or $d$), $\bar{\varepsilon}$ is found to be proportional to $d^2 u_{jet}^3/D^3$ (e.g., References [37] and [39]) or to $u_{jet}^3/d$ (e.g., Reference [46]), respectively. Also pressure drop measurements,[128] chemical tracer tests,[30] or simulations (see Section 3.2.1) can be conducted to extract local or average $\varepsilon$.

Dissipation rates in CIJs exceed those in stirred tanks by a factor of 100 to 1000,[29,128] see Table 2, with maximum dissipation occurring at the impingement point, that is, the vortex core,[60] and gradually decreasing radially and axially.[82,128] Local maxima in $\varepsilon$ near the impingement point are the result of flapping and vortex shedding,[82] shown in Figure 10. Schaer et al. [30] compared local dissipation rates of a submerged IJM with those of an impeller in a stirred tank. If properly positioned, local $\varepsilon$ from IJMs are far higher than $\varepsilon$ from the impeller, thereby showcasing the potential of submerged IJMs to create localized zones of elevated $\varepsilon$ in stirred tanks.[30,105]

## 4.4 | Mixing time analysis

While chemical tracer tests result in a segregation index,[25] calculating Da in Equation (1) requires an unambiguous value for $\tau_{mixing}$.[122] As outlined in Section 1, this is best done through the use of a micromixing time model.[25] As the exact functional relationship of $\tau_{mixing}$ continues to be debated,[29] a concise overview of select scaling relationships is given here.

In the lamellar approach, a value for the striation thickness $s$ in Equation (3) is sought (either mathematically[28,39,186] or experimentally[8,28,38,39]). Given that discussions concerning $s$ are scarce in the recent literature, this discussion is kept concise, but it is worth noting that several models have been derived for IJMs.[8,28,36,39,186] They predict, for instance, a change in $s$ proportional to $Re^{-3/4}$[36] or $Re^{-1/2}$.[28] The model developed by Baldyga and Bourne[39] is unique in the sense that it does not explicitly depend on Re and that it calculates a distribution of $s$ due to the incorporation of an exponential residence time distribution in the top of the mixing chamber, whereas other models[28,36,186] only result in a single striation value.[37,187] Laminar lamellae stretching models estimate $s$ around 10 $\mu$m (for $100 < Re < 500$), while models based on turbulent mixing suggest a value around 100 $\mu$m (for $100 < Re < 500$).[8] Fonte et al. [8] compared these predictions with experimental data from flow pattern

experiments, see Figure 9, and identified the model proposed by Lee et al. ,[28]

$$s = \left[ \frac{2\left(1 + \left(\frac{u_{jet,1}}{u_{jet,2}}\right)^{-1}\right)d^5}{2D^3} \right]^{1/2} Re^{-1/2}, \tag{36}$$

as the most physically grounded. Substituting Equation (36) into Equation (3), results in

$$\tau_{mixing} \propto \frac{d\upsilon}{(D/d)^{-3} u_{jet}}, \tag{37}$$

assuming molecular diffusion.

Assuming rapid formation of the lamellar microstructure through turbulent mixing,[29] Equation (2) can be substituted into Equation (4), thereby expressing $\tau_{mixing}$ in terms of $\varepsilon$. Assuming inelastic collisions, equal momentum of the two jets, identical physical properties of the streams, and the characteristic dimension equal to $D$ yields

$$\tau_{mixing} \propto \begin{cases} \dfrac{\upsilon^{3/2}(D/d)^{3/2}d^{1/2}}{u_{jet}^{3/2}D_i} & \text{for molecular diffusion} \\[2ex] \dfrac{\upsilon^{1/2}(D/d)^{3/2}d^{1/2}}{u_{jet}^{3/2}} & \text{for convective diffusion} \end{cases}, \tag{38}$$

for molecular diffusion (with $D_i$ the molecular diffusivity) and for momentum diffusion, respectively.[23,29]

Liu et al. [50] have shown using numerical simulations (later confirmed experimentally[46]) for $Re > 1000$ in a typical CIJ (e.g., $D/d = 4.76$, $D = 2.38$ mm[50]) that mesomixing cannot be ignored. As such, it is more appropriate to use the Corrsin's relationship,[46]

$$\tau_{mixing} \propto \begin{cases} \left[ K_1\left(\dfrac{d}{u_{jet}}\right) + K_2\left(\dfrac{d^{1/2}\upsilon^{1/2}}{u_{jet}^{3/2}}\right)\right]\ln Sc & \text{for characteristic size} = d \\[2ex] \left[ K_1\left(\dfrac{D}{u_{jet}}\right) + K_2\left(\dfrac{D^{3/2}\upsilon^{1/2}}{u_{jet}^{3/2}d}\right)\right]\ln Sc & \text{for characteristic size} = D \end{cases}, \tag{39}$$

assuming that the initial scale of segregation is $d/2$ and with $K_2 = K_1^{3/2}/2\sqrt{2}$ as proportionality constants.

Literature on IJMs discusses the influence of $u_{jet}$ predominantly in terms of Re, see Section 4.1. Most scaling relationships, including Equations (37)–(39), predict $\tau_{mixing}$ to vary proportionally with either $u_{jet}^{-1}$ or $u_{jet}^{-3/2}$, which is consistent with experimental findings.[23,28,29,46] Mixing times evaluated from CFD simulations, also taking into account mesomixing, exhibited a dependency close to $-1$.[53] The impact of geometric parameters ($d$, $D$) on $\tau_{mixing}$ is less clearly defined in the literature, but remains important to consider for scale-up considerations.[29]

All functional relationships shown in Equations (37) and (38) show a dependency of $\tau_{mixing}$ on $\upsilon$ with exponents ranging from 1/2 to 3/2. By changing $\upsilon_o$, see Figure 1, from 2.0 to 7.1 mPa·s, Johnson and Prud'homme[29] showed that convective diffusion, as opposed to

molecular diffusion, dominates in CIJs ($d = 0.25$ to $1.0$ mm, $D = 1.19$ to $4.76$ mm). Results from Gillian and Kirwan[46] in a CIJ ($d = 0.5$ mm, $D = 2.38$ mm) suggest the same modest dependency: both streams could still be mixed in the order of 10 ms when the viscosity increased from $2.3 \times 10^{-6}$ to $7.0 \times 10^{-6}$ m$^2$/s. Nunes et al.[24] confirmed this finding that molecular diffusion dominates: mixing times of 100 ms for fluids with viscosities up to 20 mPa·s were found in a CIJ ($d = 1.50$ mm, $D = 10.00$ mm). In the experiments conducted by Shi et al.,[104] it was observed that an increase in fluid viscosity (i.e., comparing water and glycerol-water solutions) did not significantly alter the mixing quality for Re ranging from 100 to 500 in a CIJ ($d = 4.20$ mm and $D = 20.08$ mm). All of the above suggests that an exponent of 0.5 is most appropriate to take into account the effect of viscosity.[29,46] Lastly, Wood et al.[80] compared the self-induced oscillatory behavior for outlet streams with viscosities of 27 and 55 cP through a spectral analysis of velocity time series, see Section 4.2. Their findings indicate that the frequency of velocity oscillations (measured at four jet diameters above the impingement point) increases with higher viscosity (at Re $= 125$).[80] However, regardless of the solvent's viscosity, the calculated St values for the characteristic frequencies remain relatively consistent.[80] This result is further corroborated by Johnson and Wood.[81]

Johnson and Prud'homme[29] also outlined a methodology to determine the absolute mixing time ($\tau_{\text{mixing}}$) by identifying a prefactor ($K_{\text{IJM}}$) for Equations (37)–(39) using chemical tracer tests. It is assumed that the relationship between Da $= \tau_{\text{mixing}}/\tau_{\text{reaction}}$ and the observed selectivity ($X$, see Equation 11) is unique.[29] For plotting $X$ against Da no knowledge of $K_{\text{IJM}}$ is required. If the scaling relationship for $\tau_{\text{mixing}}$, for example, Equations (37) and (38), predicts the mixing behavior correctly this plot should yield a straight line and individual curves for different process conditions and IJM geometries should overlap.[29] By adjusting the outlet configuration and Re, the point where the selectivity is no longer affected can be identified.[29] At that point, the mixing time is taken as equal to the residence time, and the Da is set to 1.[29] Both Johnson and Prud'homme, as well as Mahajan and Kirwan set Da $= 1$ for $X \approx 0.05$, for which Gillian and Kirwan[46] later gave a justification using a micromixing model. In Johnson and Prud'homme's study,[29] the scaling model for convective diffusion, see Equation (39), scaled well for reaction rates ranging from 340 to 9 ms, but proved inadequate when applied to reaction rates of 6.5 ms and lower. Gillian and Kirwan[46] found mixing times in the order of 10 ms in their CIJ and concluded that mixing in T-jet mixers is comparable in terms of mixing time. Lince et al.[53,56] confirmed that similar mixing times can be achieved in CIJs and T-jets, but also showed that CIJs outperform T-jet mixers when compared at the same power consumption levels.

Comparing mixing times in CIJs with residence times at the chamber outlet allows for assessing the mixing completeness in the exiting product.[56,82] However, research focused on residence time distributions in IJMs remains limited.[82,188,189] Hao et al.[82] demonstrated that increasing Re within the range of 200–1000 resulted in slight increases in residence times due to the emergence of more intricate flow patterns.

# 5 | OPERATIONAL PERFORMANCE CONSIDERATIONS

Many of the operational challenges associated with IJMs have persisted for several decades. This section discusses some operational performance considerations.

## 5.1 | Relative jet momentum

The mixing performance of IJMs hinges on the proper operation in the chaotic regime with the impingement point oscillating around the mixing chamber axis.[60] Upon mixing of two streams with different properties, or flow rates, a common requirement in many applications, the impingement location can shift considerably. Excessive impingement location movement towards one of the nozzles can cause issues: mixing oscillations are dampened, thus compromising IJMs' mixing performance, and when solids are formed they can clog an inlet nozzle.[27,69,78] Extensive research has emphasized the significance of maintaining the relative momentum of the two jets (or other related parameters) close to unity to maintain the impingement point near the center axis.[8,11,24,36,66,69] Several ratio's have been proposed to assess the balance between the two jets. For instance, the momentum ratio number ($\phi_M$),

$$\phi_M = \frac{\rho_1 d_1^2 u_{\text{jet},1}^2}{\rho_2 d_2^2 u_{\text{jet},2}^2}, \tag{40}$$

determines the relative momentum of the two jets at the moment of collision.[11,60] Another such ratio is the flow rate ratio of the two jets[60] ($\phi_{FR}$),

$$\phi_{FR} = \frac{\rho_1 u_{\text{jet},1} d_1^2}{\rho_1 u_{\text{jet},1} d_1^2}. \tag{41}$$

Fonte et al.[69] showed that the kinetic energy rate of both jets ($\phi_K$),

$$\phi_K = \frac{\rho_1^2 u_{\text{jet},1}^3 d_1^2}{\rho_1^2 u_{\text{jet},1}^3 d_1^2}, \tag{42}$$

must be balanced for optimal mixing performance, thus serving as a better predictor than $\phi_M$ or $\phi_{FR}$. This equation implies that, for increasing Re, CIJs become increasingly sensitive to small variations in the flow rates.[69] Figure 12 shows a velocity field as a function of different kinetic energy feeding ratios in a CIJ.[69] As $\phi_K$ deviates from unity, the impingement point shifts towards the jet wall with lower kinetic energy and the mixing effectiveness drops.[69] A study by Brito et al.[27] underscores the detrimental impact on the flow hydrodynamics when the equilibrium is disrupted.

The iso-momentum/iso-kinetic energy requirements thus pose the most significant limitations in IJM applications.[8,9,11,27] As stated in Section 2, MIVMs have been developed to overcome this
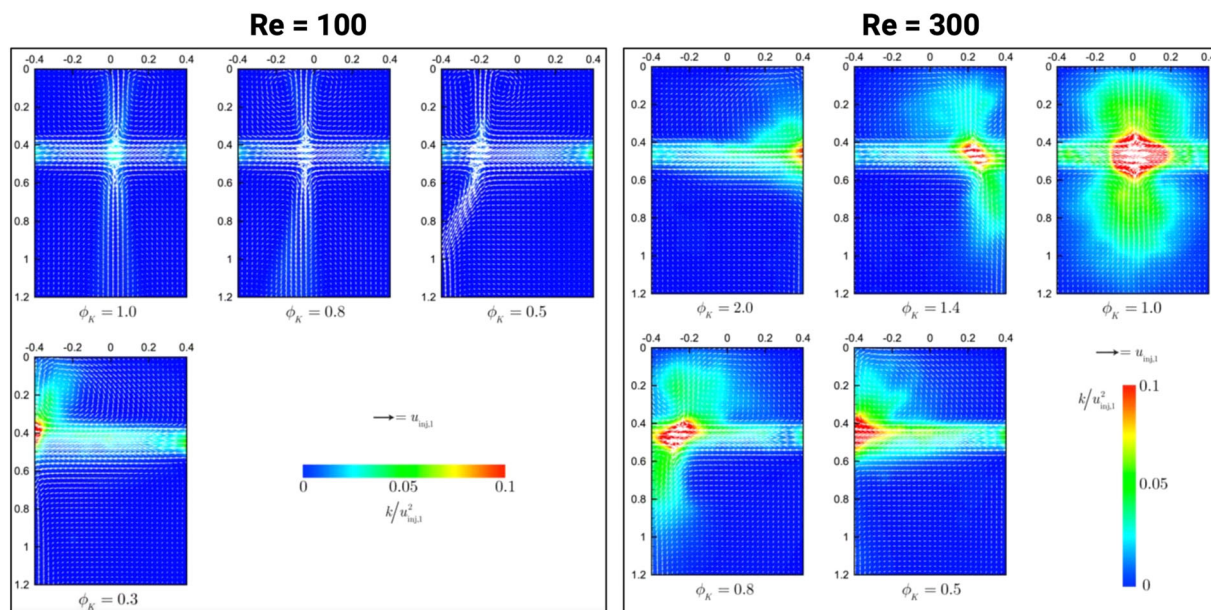
**FIGURE 12** Velocity field vector maps and nondimensional velocity fluctuations and contours as a function of the kinetic energy ratio ($\phi_K$) for Re 100 and 300 in a CIJ ($D/d = 6.66$, $D = 10$ mm). Adapted from Fonte et al. .[69] ©2016 American Institute of Chemical Engineers (AIChE).

limitation. However, some studies suggest otherwise: Tucker III and Suh[36] proposed that $\phi_M$ does not really affect mixing quality, but this statement likely reflects the technical limitations of their time. More recently, Siddiqui et al. [128] demonstrated that uneven flow conditions may not always be as detrimental as previously thought, as evidenced by stable energy dissipation and reaction yields despite a 30% flow rate disparity.[128] Notably, these observations were made at high Re (up to 6600[128]), which could influence the conclusions drawn.

### 5.1.1 | Jets' alignment

When flow rate ratios and properties are dictated by process specifications, achieving the iso-momentum/iso-kinetic energy condition with a typical IJM necessitates the use of injectors with different diameters.[8,85] Another option is to adjust the jets' alignment to prevent one fluid stream from pushing the impingement point to the nozzle of the other fluid stream, thereby enhancing the robustness of the process.[26,27,78]

Liu et al. [78,190] compared jets angled 10° downward and parallel alignment of the jets for a submerged IJM in a stirred tank. They also investigated the more uncommon 10° upward alignment.[190] Their results indicated that the 10° downward alignment gave the best results.[190] In a CIJ with upward-angled inlets, the jets converge at the mixing chamber's top and then accelerate downwards: the proximity of the top wall restricts the impingement point's free oscillation, hindering effective mixing due to less vortex formation.[88] With downward-angled inlets, the jets are not colliding directly either and the characteristic size of the pancake core, see

Section 4, is reduced,[88] which also reduces mixing performance. This was confirmed by Metzger and Kind's[26] work in a CIJ ($d = 0.50$ mm, $D = 2.00$ mm, without chamber headspace) with the jets downward-aligned at 0° and at 15°, which showed that in the angled configuration the mixing behavior is more fixed as there are less oscillations in the inlet jet streams. Unger and Muzzio[85] also conducted a study on the impact of asymmetric jet geometry without direct impingement for Re between 150 and 600. In their configuration, the streams flow adjacent to each other and impinge on the opposite wall instead.[85] This results in notably inferior mixing, characterized by a steady-state swirling motion at the bottom of the mixer,[85] and should thus be avoided. It is worth pointing out that Unger and Muzzio's[85] experiments were conducted in a setup characterized by notably larger dimensions ($d = 12.70$ mm, $D = 88.90$ mm) compared to typical CIJs.

### 5.1.2 | Mixing fluids with dissimilar viscosities

Equation (42) does not explicitly consider the influence of mixing fluids with different viscosities. Demyanovich and Bourne's[72] result for impingement mixing of liquid sheets suggest that up to a certain threshold, mixing reactants of unequal viscosities can be assumed to occur at a uniform viscosity equal to that of the resulting product. Wang et al. [20] have shown that, once the viscosity ratio of the two jets being mixed exceeds 3, the mixing becomes significantly worse. Brito et al. [27] illustrated that for viscosity ratios of 2, mixing in a CIJ ($D/d = 6.66$, $D = 10.00$ mm) in the chaotic regime can still form thin lamellae and provide good mixing, see Figure 13, as long as the jets are balanced.

**Re = 100**
$\mu_1 = 0.04$ Pa s, $\mu_2 = 0.02$ Pa s



$\phi_K = 0.2$     $\phi_K = 0.5$     $\phi_K = 1.0$     $\phi_K = 2.0$     $\phi_K = 5.0$

**Re = 125**
$\mu_1 = 0.04$ Pa s, $\mu_2 = 0.02$ Pa s



$\phi_K = 0.2$     $\phi_K = 0.67$     $\phi_K = 1.0$     $\phi_K = 1.5$     $\phi_K = 5.0$

**Re = 150**
$\mu_1 = 0.04$ Pa s, $\mu_2 = 0.02$ Pa s



$\phi_K = 0.2$     $\phi_K = 0.5$     $\phi_K = 1.0$     $\phi_K = 1.5$     $\phi_K = 5.0$
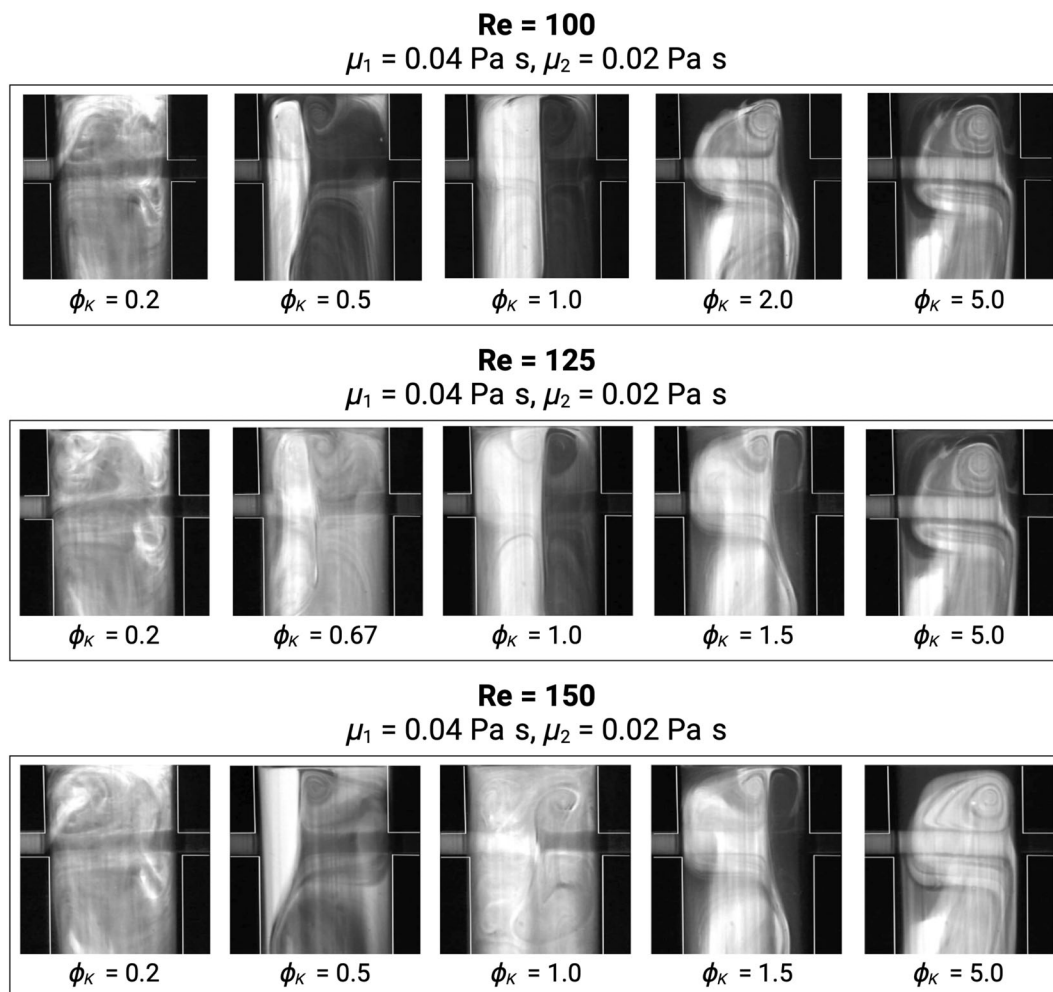
**FIGURE 13** Visualization (with planar laser-induced fluorescence) of flow patterns generated at the impingement zone through the mixing of two streams with different viscosities in a confined impinging jet mixer (CIJ) chamber ($D/d = 6.66$, $D = 10.00$ mm) across various kinetic energy ratios ($\phi_K$) for Re of 100, 125, and 150. The critical Reynolds number was identified at 111. For increasing $\phi_K$, the impingement point is pushed away from the chamber axis. Adapted from Brito et al. .[27] ©2018 Institution of Chemical Engineers. Published by Elsevier B.V. All rights reserved.

## 5.2 | Impingement point tracking

To operate IJMs optimally, tight control is essential. As Re increases, IJMs become progressively more sensitive to even minor deviations in jet flow rates and it becomes increasingly harder to maintain the impingement point in the center.[69] Controlling and monitoring mixing performance is difficult to a lack of good control variables. As a result indirect measurements, that have a slow response to changes in mixing, for example, temperature,[28,38,43] are used.[61] One notable exception is the monitoring of static pressure frequencies.[61] Another, more prevalent, approach is to track the impingement point position, for example, to validate whether the iso-momentum condition is satisfied.[24,60]

The impingement point exhibits sudden shifts.[82] In gaseous IJMs, for $2 < D/d < 8$, significant shifts in the impingement point occur. Particularly at $D/d = 4.8$ and $D/d = 6.67$, two common configurations in CIJs, the impingement point is highly unstable.[84,178,179] A deviation of just 10% in the momentum balance can shift the impinging point

entirely to one injector nozzle.[9,66] Erkoç et al.[61] showed that the velocity component along the jets' inlet axis (at the impingement point) showed a close synchronisation of local maxima with a time series of the static pressure difference of the two inlet jets. A spectral analysis, see Section 4.2, illustrates how both the velocity component at the impingement point and the static pressure difference in the feed lines have comparable typical frequencies, $\phi$. This implies that the pressure signal frequency is related to the flow structures in the mixing zone.[61] More specifically, the typical frequencies associated with the vortex shedding around the impingement point, see Section 4.2, can be controlled in real time by measuring static pressure at the jets feeding lines.[65,88]

Three analytical models have been developed to track the impingement point: the elastic analogue model (EAM),[69] the jets kinetic energy model (KEM),[60] and the jets momentum model (JMM).[60] These models are expressed in terms of the dimensionless impingement point position[60,69] ($\xi = x_{IP}/(D/2)$),

$$\xi = \begin{cases} \dfrac{\left(\dfrac{Re_2}{10}\dfrac{d_2}{D}+1\right)\sqrt{\phi_K \dfrac{Re_1}{Re_2}\dfrac{d_1}{d_2}} - \left(\dfrac{Re_1}{10}\cdot\dfrac{d_1}{D}+1\right)}{\sqrt{\phi_K \dfrac{Re_1}{Re_2}\cdot\dfrac{d_1}{d_2}}+1} & \text{EAM} \\[3em] \dfrac{\left(\dfrac{\rho_1^{1/2}}{\rho_2^{1/2}}\phi_M\dfrac{v_2}{v_1}\right)\left(1+\dfrac{Re_2}{8}\dfrac{d_2}{D}\right) - \left(1+\dfrac{Re_1}{8}\dfrac{d_1}{D}\right)}{\dfrac{\rho_1^{1/2}}{\rho_2^{1/2}}\phi_M\dfrac{v_2}{v_1}+1} & \text{KEM}, \\[3em] \dfrac{\left(\dfrac{\rho_1}{\rho_2}\phi_M\dfrac{v_2}{v_1}\right)\left(1+\dfrac{Re_2}{8}\dfrac{d_2}{D}\right) - \left(1+\dfrac{Re_1}{8}\dfrac{d_1}{D}\right)}{\dfrac{\rho_1}{\rho_2}\phi_M\dfrac{v_2}{v_1}+1} & \text{JMM} \end{cases} \quad (43)$$

with $x_{IP}$ being the axial impingement point location. The models have been evaluated for direct impingement using PLIF and CFD data[60,69]: For viscosity ratios up to 9 and identical density ratios, the JMM model is recommended.[60] For fluids with different viscosity and density ratios, the KEM model is most appropriate,[60] while the EAM is suitable for mixing processes involving fluids with similar properties.[60]

These models illustrate the intrinsically asymmetric behavior of CIJs with respect to Re. In addition $\xi$ also shows that, for constant $\phi_K$ and increasing Re, the impingement zone moves closer to the wall of the jet with the lowest Re.[69] These models can be used to extract design equations for optimal CIJ operation.[60,69]

## 5.3 | Scale-up

In certain scenarios where an even higher throughput is desired, IJMs need to be scaled up.[29,46,53,54,58] The jet velocity has been proposed as the scaling variable in free and submerged IJMs,[23,30] but it has been shown in CIJs that this is not sufficient to maintain consistent conversions.[29,54] To achieve Da similitude across scales, geometric corrections are required.[29] A pragmatic approach involves utilizing the $\tau_{mixing}$ relationships outlined in Equations (37)–(39), complemented by an additional velocity correction,[29]

$$u_{\text{jet, large scale}} = u_{\text{jet, small scale}}\left(\dfrac{d_{\text{large scale}}}{d_{\text{small scale}}}\right). \quad (44)$$

For example, utilizing this relationship with $\tau_{mixing} \propto d^{0.5}/u_{jet}^{-1.5}$ leads to a scale-up criterion in terms of the nozzle diameter,

$$\dfrac{d_{\text{large scale}}}{d_{\text{small scale}}} = \left(\dfrac{Q_{\text{large scale}}}{Q_{\text{small scale}}}\right)^{3/7}, \quad (45)$$

where Q represents the volumetric flow rate.[46]

## 5.4 | Limitations

One constraint associated with IJMs is the significant pressure drop incurred when pumping high volumetric flow rates through the mm-sized nozzles,[26,36,56] potentially leading to substantial pumping

costs.[26] However, this drawback is somewhat balanced by the low capital cost associated with typical IJM setups.[15,31]

In addition, there are some potential operational limitations when using IJMs. The iso-momentum/iso-kinetic requirement, see Section 5.1, is a significant limiting factor.[8,11,27,36] Moreover, maintaining the oscillatory dynamic behavior in CIJs required to achieve the best mixing performance can be challenging due to their sensitivity (e.g., impingement instability) and inherent randomness at high Re.[84] For example, dynamic oscillations may induce pressure fluctuations, resulting in oscillatory pumping behavior which disrupts the process.[26] Coupled with the complexity of *in situ* analysis and control of the mixing behavior, these operational challenges may prevent IJMs' usage.

# 6 | APPLICATIONS

With the widespread adoption of IJMs, see Figure 2, delving into specific applications becomes impractical. To underscore their versatility and efficacy, two categories of applications closely associated with IJMs are discussed: liquid and particulate processing. The former refers to processes where the output stream remains fully liquid postmixing, while the latter deals with applications where solid particles are formed upon jet impingement, resulting in an output stream with solid particles in a liquid medium.

## 6.1 | Liquid processing

### 6.1.1 | Reaction injection molding

The initial development of CIJs was specifically tailored for reaction injection molding (RIM) applications.[11,28,35,36] RIM is a polymer production method where highly viscous reactive liquid monomers, called pre-polymers, are mixed and injected into a mould to undergo polymerization.[8–11] RIM is widely used to fabricate plastic components for various industries (e.g., automotive, sporting goods, and household appliances).[10,191] RIM processes can be operated at low temperatures and relatively low pressure requirements, such that the energy cost per volume of material is also low.[10] The primary polymer produced via RIM is polyurethane synthesized from mixing polyol (typical $v$ of 0.1 Pa·s[60]) and isocyanate (typical $v$ of 1 Pa·s[60]).[10,11,28,36]

When $\tau_{mixing}$ is longer than the resin system's gel time, it can result in unreacted monomers compromising product quality.[36] CIJs are the best technology to overcome challenges posed by the mixing of two highly viscous streams, which cannot be effectively achieved in conventional equipment, see Table 2, at high flow rates (up to 3 kg/s, e.g., References 11 and 36), ensuring fast curing and optimal product quality.[8,36,42,81,192]

### 6.1.2 | Liquid-liquid extraction and emulsification

IJMs are used for mixing two miscible streams (e.g., References 8,11,23,27–29,36,37, and 80). However, in certain applications CIJs

have also been utilized for mixing two immiscible streams, and in such instances they are more aptly referred to as impinging jet contactors [79,193–196]. For instance, impinging jet contactors enable high volumetric production of monodisperse emulsions with a tight size distribution (e.g.,[185,197–199]), crucial in sectors like food, paint, and pharmaceuticals,[199,200] whereas existing technologies are hindered by their low throughput or poor contacting performance[200]

Upon the collision of two immiscible jets, one fluid becomes emulsified within the other, forming droplets. This process is influenced by various factors such as local mixing dynamics, shear forces, mixing geometry, and physical properties of the fluids, resulting in a competition between droplet breakup and coalescence.[199] In the absence of heterogeneous reactions, the mechanisms involved are akin to mixing processes, as the primary objective is usually to enhance interfacial contact. As impinging jet contactors have orders of magnitude higher localized energy dissipation rates than conventional contactors,[193,197] also the interfacial area created upon jet impingement is significantly higher.[195] For the same reason, impinging jet contactors also prove useful for liquid-liquid extraction processes in various processes.[193,195,196,201–203]

## 6.2 | Particulate processing

### 6.2.1 | Precipitation and crystallization

Precipitation/crystallization of one or more solutes from solution requires the generation of a supersaturated solution which can be achieved through multiple mechanisms such as (A) addition of an antisolvent, (B) lowering the mixture temperature (see Reference 160 for a theoretical discussion of temperature-induced nucleation in IJMs), and (C) *in situ* reaction of soluble precursors to form an insoluble product. It is possible to combine two or more mechanisms in a given process (e.g., see Reference 15). The rapid and intense mixing that IJMs provide enable the mixture to rapidly become nearly spatially homogeneous with a high supersaturation, prior to the onset of nucleation[204] (which is dominated by primary nucleation[205]). The use of IJMs enables the production of small particles with a narrow size distribution.[206] Important particle attributes such as the size and morphology can be tuned further by changing the hydrodynamic, operating, and feed conditions of the IJM (e.g., see Reference 207). IJMs also provide a scalable and reproducible (by virtue of steady-state operation) production platform which is important for meeting market demands and product quality requirements.

Midler et al.,[208] in a patent assigned to Merck & Co. Inc., were the first to employ IJMs for crystallizing pharmaceutical particles, resulting in crystals ranging from 5 to 20 $\mu$m and simultaneously enhancing purity. Since then, IJMs have found application in the production of micro- and/or nanoparticles by precipitation in a "bottom-up" manner for pharmaceutical applications (e.g., see References 12–14,19,21,57,208–211). The production of drug nanoparticles/nanocrystals confers several desirable properties to the product such as enhanced dissolution characteristics and bioavailabilty, improved drug delivery, and enabling the development of novel formulations.[212] Compared to "top-down" approaches (i.e., breaking down a larger particle into smaller particles) such as high-pressure homogenization,[213] "bottom-up" approaches offer multiple advantages such as significantly lower energy/pressure input requirements, gentler processing of labile species, and lower contamination risks.[214] IJMs have also found application in the production of larger drug substance crystals during secondary manufacturing[215] either being used directly,[15,18,20] or as a platform for the continuous generation of seeds which are then fed into a downstream crystallizer.[16,17,21] Avenues for process intensification, facilitated by IJMs, have also been explored such as integrating reaction steps with crystallization[190] and directly purifying reaction mixtures.[97]

IJMs have also found extensive use in the production of a wide range inorganic/metal nanoparticles, typically produced by reactive precipitation involving two or more streams containing soluble precursors. Examples of nanoparticles (with exemplar applications in parenthesis) produced using IJMs include calcium carbonate (pigments, fillers, multiple biomedical applications),[207,216] gadolinium orthoferrite (catalysis, MRI contrast agent),[217] silver (antimicrobials, solar cells),[218,219] and nickel (catalysis).[220] Inorganic systems also provide an excellent framework for conducting more fundamental work on IJM process development (e.g., see Reference 221), understanding precipitation/crystallization nucleation and growth (e.g., see Reference 222), and developing mathematical models of the precipitation process (e.g., see Reference 223).

### 6.2.2 | Complex nanomaterials and nanoformulations

Motivated by similar reasons outlined in Section 6.2.1, CIJs and MIVMs have also found significant application in the production of complex nanomaterials and nanoformulations. While this technology has become established with multiple patents being issued for a range of complex products (e.g., see References 224–228), continued innovation into developing new products and/or use-cases is actively underway. The interested reader is referred to the excellent reviews[229,230] for an in-depth discussion of flash nanoprecipitation/nanocomplexation and its use in the production of various nanoformulations.

Broadly, two categories of applications for complex products have emerged: (A) Encapsulation/loading of one or more species of interest into a nanoparticle/nanocarrier. Typically, the species of interest, for example, a therapeutic compound, is encapsulated in a wall material (a wide range of wall materials for example, polymers, lipids, and silica have been used) to achieve a variety of goals such as controlled drug delivery and/or protection of labile species. Various examples can be found in Reference 230 and citations therein. The most notable recent example, and the largest commercial application, was the use of CIJs and MIVMs in the large-scale production of lipid nanoparticles encapsulating mRNA for COVID-19 vaccines.[231] (B) Formation of nanomaterials with complex nanostructures either for direct application due to improved functionality (e.g., electrochemical/catalytic activity),[232–234]

or by producing structures that can serve as templates for subsequent applications.[235,236]

# 7 | FUTURE PERSPECTIVES

The next phase of development for IJMs should focus on enhancing process control by integrating characterization tools for *in situ* and/or real-time monitoring of mixing dynamics across various applications. These tools necessitate exceptional spatial and temporal resolution, coupled with the capacity to discern the different liquid phases and/or detect the presence of nanoparticles, see Section 6.

For the latter, optical techniques, particularly those based on light scattering and high-speed (microscopy) imaging, show promise. For instance, a recently developed noninvasive real-time monitoring method, relying on speckle analysis with a physics-enhanced autocorrelation-based estimator (PEACE),[237] has demonstrated potential in extracting particle size distributions. While current capabilities are limited to micron-sized particles,[237] ongoing advancements may overcome these constraints, rendering the technique suitable for monitoring applications in IJMs. Along the same lines, the integration of dynamic light scattering (DLS) into IJMs holds potential and warrants further exploration. DLS presents a methodology for real-time monitoring of particle size distribution and concentration changes, distinguishing itself with its online and noninvasive capabilities. However, existing theoretical foundations primarily address the Brownian motion of freely moving particles, neglecting the complexities of ordered particle motion commonly encountered in industrial applications. This theoretical limitation poses significant challenges, particularly in scenarios where particle behavior deviates from idealized diffusion dynamics, as is the case in IJMs. In contrast to conventional solid particle size detection methods, which often necessitate offline measurements, DLS offers the advantage of continuous in situ monitoring. To advance the efficacy of DLS for industrial IJMs' applications, future research should focus on the development of theoretical models that incorporate various particle motions and interactions. Such advancements promise to increase the technique's applicability and precision, thereby facilitating more robust process control and monitoring protocols. Furthermore, enhancements in the temporal resolution of DLS measurements can enable more precise real-time monitoring of particle dynamics and mixing within IJMs, emphasizing the potential for expanded utility across a broad spectrum of industrial processes.

Another promising trajectory is to leverage the advantages of hyperspectral imaging (HSI) technology for differentiating between various liquid phases based on their spectral characteristics. HSI combines the advantages of both spectroscopy and modern imaging methods by capturing a large number of images over continuous and numerous spectral bands covering a wide range of wavelengths from mid-infrared and near-infrared to visible segments of the electromagnetic spectrum.[238] Characterized by high spectral/spatial/temporal resolution imaging capabilities, HSI is a sensitive tool able to detect subtle spectral variations which can be used for characterizing the fast-flow environment around the impingement point. Through the identification and change of unique chemical spectral signatures, HSI has the potential to quantify mixing even in systems with overlapping spectral emissions or reflections, a common challenge in chemical and pharmaceutical processes. By combining HSI with advanced artificial intelligence tools, the instantaneous extraction of valuable characterization insights from extensive HSI datasets becomes achievable. HSI has already been successfully applied as a fast and accurate characterization tool for flow-field measurements and dynamics characterization.[239]

In addition to the discussed examples, also other noninvasive monitoring techniques, such as high-speed imaging and high-speed electrical impedance tomography, may proof to be viable options for integration into IJMs.

# 8 | CONCLUDING REMARKS

IJMs are a staple technology for achieving rapid and efficient mixing. By colliding two liquid colinear jets head-on within a typically confined, that is, confined impinging jet mixer (CIJ) volume, IJMs offer mixing times in the order of ms, surpassing conventional mixing equipment. This review provides an overview of IJMs, covering technology and design, characterization methods, mixing behavior, performance considerations, and application examples.

Despite their widespread adoption, challenges persist, notably in understanding the dynamic mixing behavior and integrating effective process control measures. The continued advancement of IJMs hinges on addressing these challenges. As new applications will continue to emerge with increasingly challenging process and restrictive regulatory requirements, for example, as seen recently with the demand for fast and reproducible production of complex nanoformulations for novel therapeutics, the imperative for innovative research and development in this field will only intensify. This review has taken the first step by summarizing the extensive knowledge on this topic and by providing a trajectory for future research.

## NOMENCLATURE: LATIN SYMBOLS

| | |
|---|---|
| $C$ | concentration as per convention |
| $d$ | nozzle diameter (m) |
| $D$ | chamber diameter (m) |
| $D_{ns}$ | internozzle separation (m) |
| $D_{tank}$ | tank diameter (m) |
| $D_i$ | molecular diffusivity ($m^2\,s^{-1}$) |
| $f_\xi$ | composition PDF (–) |
| $h$ | chamber dome height (m) |
| $H$ | chamber height (m) |
| $K$ | proportionality constant (–) |
| $L_s$ | initial segregation thickness (m) |
| $p$ | pressure ($kg\,m^{-1}s^{-2}$) |
| $Q$ | volumetric flow rate ($m^3\,s^{-1}$) |
| $s$ | striation thickness (m) |
| $T$ | temperature (K) |

| | |
|---|---|
| $t$ | time (s) |
| $u_{jet}$ | velocity of jet (K) |
| $V$ | volume (m$^3$) |
| $V_m$ | mesomixing volume (m$^3$) |
| $w$ | chamber width (m) |
| $x_{IP}$ | axial impingement point (m) |

## GREEK SYMBOLS

| | |
|---|---|
| $\tau_{mixing}$ | mixing time (s) |
| $\tau_{reaction}$ | reaction time (s) |
| $\rho$ | density (s) |
| $\eta$ | dynamic viscosity (kg m$^{-1}\cdot$s$^{-1}$) |
| $\upsilon$ | kinematic viscosity (m$^2\cdot$s$^{-1}$) |
| $\varepsilon$ | energy dissipation rate (W kg$^{-1}$) |
| $\lambda$ | Kolmogorov length scale (m) |
| $\lambda_B$ | Batchelor length scale (m) |
| $\theta$ | angle alignment (°) |
| $\sigma^2$ | variance (–) |
| $\xi_i$ | concentration of $i$th scalar as per convention |
| $\phi$ | typical oscillation frequency (s$^{-1}$) |
| $\psi$ | stream function (kg m$^{-1}\cdot$s$^{-1}$) |
| $\varphi$ | velocity potential (m$^2\cdot$ s$^{-1}$) |
| $\Omega$ | vorticity function (s$^{-1}$) |

## DIMENSIONLESS NUMBERSSYMBOL DESCRIPTION

| | |
|---|---|
| Da | Damköhler number |
| Re | Reynolds number |
| St | Strouhal number |
| Sc | Schmidt number |
| $\phi_M$ | momentum ratio number |
| $\phi_{FR}$ | flow rate ratio |
| $\phi_K$ | kinetic energy ratio |
| $I_s$ | intensity of segregation |
| $X$ | segregation index |
| $t^*$ | dimensionless time |
| $\xi$ | dimensionless impingement point position |

## SUBSCRIPTS

| | |
|---|---|
| crit | critical |
| in | inlet |
| $i$ | species i |
| o | outlet |

## AUTHOR CONTRIBUTIONS

**Cedric Devos:** conceptualization; writing – original draft; investigation. **Saikat Mukherjee:** investigation; writing – original draft. **Pavan Inguva:** investigation; writing – original draft. **Shalini Singh:** investigation; writing – original draft. **Yi Wei:** investigation; writing – original draft. **Sandip Mondal:** investigation; writing – original draft. **Huiwen Yu:** investigation; writing – original draft. **George Barbastathis:** writing – review and editing; supervision. **Torsten Stelzer:** writing – review and editing; supervision. **Richard D. Braatz:** supervision; writing – review and editing; funding acquisition. **Allan S. Myerson:** writing – review and editing; supervision; conceptualization; funding acquisition.

## CONFLICT OF INTEREST STATEMENT

The authors declare that they have no known competing financial interests or personal relationships that could have appeared to influence the work reported in this paper.

## DATA AVAILABILITY STATEMENT

Data sharing is not applicable to this article as no new data were created or analysed in this study, except for Figure 2. The data shown in Figure 2 is sourced from Web of Science (Clarivate) and can be regenerated in Web of Science using the search query provided in the caption or can be made available from the corresponding author upon reasonable request. All figures, except Figures 1, 2, and 5, are reproduced from previously published sources and therefore do not have data that can be shared. Figures 1 and 5 are schematics and do not depict specific data. The data shown in Figure 2 is sourced from Web of Science (Clarivate) and can be regenerated in Web of Science using the search query provided in the caption or can be made available from the corresponding author upon reasonable request.

## ORCID

*Cedric Devos* https://orcid.org/0000-0002-8154-4872
*Allan S. Myerson* https://orcid.org/0000-0002-7468-8093

## REFERENCES

1. Abiev RS. Impinging-jets micromixers and microreactors: state of the art and prospects for use in the chemical technology of nanomaterials (review). *Theor Found Chem Eng.* 2020;54(6):1131-1147.
2. Santos RJ, Sultan MA. State of the art of mini/micro jet reactors. *Chem Eng Technol.* 2013;36(6):937-949.
3. Tamir A, Kitron A. Applications of impinging-streams in chemical engineering processes. *Chem Eng Commun.* 1987;50(1-6):241-330.
4. Tamir A. *Impinging-Stream Reactors.* 1st ed. Elsevier; 1994.
5. Tamir A, Herskowits D, Herskowits V. Impinging Jet Absorbers. *Chem Eng Commun.* 1990;28:165–172.
6. Paul EL, Atiemo-obeng VA, Kresta SM. *Handbook of Industrial Mixing.* 1st ed. Wiley; 2003.
7. Certain data included herein are derived from Clarivate InCites. © Copyright Clarivate 2024. All rights reserved.
8. Fonte CP, Sultan MA, Santos RJ, Dias MM, Lopes JCB. Flow imbalance and Reynolds number impact on mixing in confined impinging jets. *Chem Eng J.* 2015;260:316-330.
9. Gomes NM, Fonte CP, CCe S, et al. Real time control of mixing in reaction injection moulding. *Chem Eng Res Des.* 2016;105:31-43.
10. Lee LJ. Polyurethane reaction injection molding: process, materials, and properties. *Rubber Chem Technol.* 1980;53(3):542-599.
11. Malguarnera SC, Suh NP. Liquid injection molding I. An investigation of impingement mixing. *Polym Eng Sci.* 1977;17(2):111-115.

12. Dong Y, Ng WK, Shen S, Kim S, Tan RB. Controlled antisolvent precipitation of spironolactone nanoparticles by impingement mixing. *Int J Pharm*. 2011;410(1-2):175-179.

13. Emami MS, Haghshenasfard M, Zarghami R, Sadeghi R, Esfahany MN. Experimental study on the reduction of loratadine particle size through confined liquid impinging jets. *Int J Pharm*. 2020;587:119668.

14. Han J, Zhu Z, Qian H, et al. A simple confined impingement jets mixer for flash nanoprecipitation. *J Pharm Sci*. 2012;101(10):4018-4023.

15. Jiang M, Li YED, Tung HH, Braatz RD. Effect of jet velocity on crystal size distribution from antisolvent and cooling crystallizations in a dual impinging jet mixer. *Chem Eng Process Process Intensif*. 2015;97: 242-247.

16. Jiang M, Wong MH, Zhu Z, et al. Towards achieving a flattop crystal size distribution by continuous seeding and controlled growth. *Chem Eng Sci*. 2012;77:2-9.

17. Liu WJ, Ma CY, Liu JJ, Zhang Y, Wang XZ. Continuous reactive crystallization of pharmaceuticals using impinging jet mixers. *AIChE J*. 2017;63(3):967-974.

18. Pal S, Madane K, Kulkarni AA. Antisolvent based precipitation: batch, capillary flow reactor and impinging jet reactor. *Chem Eng J*. 2019;369:1161-1171.

19. Tari T, Szabó-Révész P, Aigner Z. Comparative study of different crystallization methods in the case of cilostazol crystal habit optimization. *Crystals*. 2019;9(6):295.

20. Wang X, Gillian JM, Kirwan DJ. Quasi-emulsion precipitation of pharmaceuticals. 1. Conditions for formation and crystal nucleation and growth behavior. *Cryst Growth Des*. 2006;6(10): 2214-2227.

21. Woo XY, Tan RBH, Braatz RD. Precise tailoring of the crystal size distribution by controlled growth and continuous seeding from impinging jet crystallizers. *CrstEngComm*. 2011;13(6):2006.

22. Baldyga J, Bourne JR. *Turbulent Mixing and Chemical Reactions*. Wiley; 1999.

23. Mahajan AJ, Kirwan DJ. Micromixing effects in a two-impinging-jets precipitator. *AIChE J*. 1996;42(7):1801-1814.

24. Nunes MI, Santos RJ, Dias MM, Lopes JCB. Micromixing assessment of confined impinging jet mixers used in RIM. *Chem Eng Sci*. 2012; 74:276-286.

25. Falk L, Commenge J. Characterization of mixing and segregation in homogeneous flow systems. *Micro Process Eng*. 2013;1:145-173.

26. Metzger L, Kind M. On the transient flow characteristics in confined impinging jet mixers - CFD simulation and experimental validation. *Chem Eng Sci*. 2015;133:91-105.

27. Brito MS, Esteves LP, Fonte CP, Dias MM, Lopes JC, Santos RJ. Mixing of fluids with dissimilar viscosities in confined impinging jets. *Chem Eng Res Des*. 2018;134:392-404.

28. Lee LJ, Ottino JM, Ranz WE, Macosko CW. Impingement mixing in reaction injection molding. *Polym Eng Sci*. 1980;20(13):868-874.

29. Johnson BK, Prudhomme RK. Chemical processing and micromixing in confined impinging jets. *AIChE J*. 2003;49(9):2264-2282.

30. Schaer E, Guichardon P, Falk L, Plasari E. Determination of local energy dissipation rates in impinging jets by a chemical reaction method. *Chem Eng J*. 1999;72(2):125-138.

31. Pal S, Madane K, Mane M, Kulkarni AA. Impingement dynamics of jets in a confined impinging jet reactor. *Ind Eng Chem Res*. 2021; 60(2):969-979.

32. Myerson AS, Erdemir D, Lee AY. *Handbook of Industrial Crystallization*. 3rd ed. Cambridge University Press; 2019.

33. Liu Y, Olsen MG, Fox RO. Turbulence in a microscale planar confined impinging-jets reactor. *Lab Chip*. 2009;9(8):1110-1118.

34. Carver J, Rollman WF. Method and Apparatus for Mixing and Contacting Fluids. U.S. Patent 2,751, 335. 1956.

35. Keuerleber R, Pahl FW. Device for Feeding Flowable Material to A mold cavity. US patent 706,515. 1972.

36. Tucker CL, Suh NP. Mixing for reaction injection molding. I. Impingement mixing of liquids. *Polym Eng Sci*. 1980;20(13):875-886.

37. Kusch HA, Ottino JM, Shannon DM. Analysis of impingement mixing-reaction data: use of a lamellar model to generate fluid mixing information. *Ind Eng Chem Res*. 1989;28(3):302-315.

38. Kolodziej P, Macosko CW, Ranz WE. The influence of impingement mixing on striation thickness distribution and properties in fast polyurethane polymerization. *Polym Eng Sci*. 1982;22(6):388-392.

39. Baldyga J, Bourne JR. Distribution of striation thickness from impingement mixers in reaction injection molding. *Polym Eng Sci*. 1983;23(10):556-559.

40. Hyrmak AN, Wood PE, Johnson D. Impingement mixing of liquids in reaction injection-molding. *Annu Tech Conf Proc J*. 1991;37:2329-2333.

41. Kolodziej P, Yang WP, Macosko CW, Wellinghoff ST. Impingement mixing and its effect on the microstructure of RIM polyurethanes. *J Polym Sci B*. 1986;24(10):2359-2377.

42. Nguyen LT, Suh NP. Processing of polyurethane/polyester interpenetrating polymer networks by reaction injection molding. Part III: flow reorientation through multiple impingement. *Polym Eng Sci*. 1986;26(12):843-853.

43. Nguyen LT, Suh NP. Processing of polyurethane/polyester interpenetrating polymer networks by reaction injection molding. Part II: mixing at high reynolds numbers and impingement pressures. *Polym Eng Sci*. 1986;26(12):799-842.

44. Macosko CW, McIntyre DB. RIM Mixhead with High Pressure Recycle. US Patent 473,531. 1984.

45. Margulis K, Magdassi S, Lee HS, Macosko CW. Formation of curcumin nanoparticles by flash nanoprecipitation from emulsions. *Public Health Nutr*. 2014;434:65-70.

46. Gillian JM, Kirwan DJ. Identification and correlation of mixing times in opposed-jet mixers. *Chem Eng Commun*. 2008;195(12):1553-1574.

47. Johnson BK, Prudhomme RK. Mechanism for rapid self-assembly of block copolymer nanoparticles. *Phys Rev Lett*. 2003;91(11):1-4.

48. Icardi M, Gavi E, Marchisio DL, et al. Investigation of the flow field in a three-dimensional confined impinging jets reactor by means of microPIV and DNS. *Chem Eng J*. 2011;166(1):294-305.

49. Icardi M, Gavi E, Marchisio DL, Olsen MG, Fox RO, Lakehal D. Validation of LES predictions for turbulent flow in a confined impinging jets reactor. *App Math Model*. 2011;35(4):1591-1602.

50. Liu Y, Fox RO. CFD predictions for chemical processing in a confined impinging-jets reactor. *AIChE J*. 2006;52(2):731-744.

51. Feng H, Olsen MG, Liu Y, Fox RO, Hill JC. Investigation of turbulent mixing in a confined planar-jet reactor. *AIChE J*. 2005;51(10): 2649-2664.

52. Liu Y, Cheng C, Liu Y, Prud RK, Fox RO. Mixing in a multi-inlet vortex mixer (MIVM) for flash nano-precipitation. *Chem Eng Sci*. 2008; 63(11):2829-2842.

53. Valente I, Celasco E, Marchisio DL, Barresi AA. Nanoprecipitation in confined impinging jets mixers: production, characterization and scale-up of pegylated nanospheres and nanocapsules for pharmaceutical use. *Chem Eng Sci*. 2012;77:217-227.

54. Gavi E, Marchisio DL, Barresi AA. CFD modelling and scale-up of confined impinging jet reactors. *Chem Eng Sci*. 2007;62(8):2228-2241.

55. Marchisio DL. Large Eddy simulation of mixing and reaction in a confined impinging jets reactor. *Comput Chem Eng*. 2009;33(2): 408-420.

56. Lince F, Marchisio DL, Barresi AA. A comparative study for nanoparticle production with passive mixers via solvent-displacement: use of CFD models for optimization and design. *Chem Eng Process Process Intens*. 2011;50(4):356-368.

57. Lince F, Marchisio DL, Barresi AA. Strategies to control the particle size distribution of poly-ε-caprolactone nanoparticles for pharmaceutical applications. *J Colloid Interface Sci*. 2008;322(2):505-515.

58. Marchisio DL, Rivautella L, Barresi AA. Design and scale-up of chemical reactors for nanoparticle precipitation. *AIChE J*. 2006;52(5): 1877-1887.

59. Santos RJ, Teixeira AM, Costa MR, Lopes JC. Operational and design study of RIM machines. *Int Polym Process*. 2002;17(4):387-394.

60. Brito MS, Dias MM, Lopes JC, Santos RJ, Fonte CP. A general design equation for confined impinging jets mixers. *Chem Eng J*. 2023;465-(April):142892.

61. Erkoç E, Santos RJ, Nunes MI, Dias MM, Lopes JCB. Mixing dynamics control in RIM machines. *Chem Eng Sci*. 2007;62(18-20):5276-5281.

62. Erkoç E, Fonte CP, Dias MM, Lopes JCB, Santos RJ. Numerical study of active mixing over a dynamic flow field in a T-jets mixer-induction of resonance. *Chem Eng Res Des*. 2016;106:74-91.

63. Santos RJ, Teixeira AM, Lopes JCB. Study of mixing and chemical reaction in RIM. *Chem Eng Sci*. 2005;60(8-9):2381-2398.

64. Santos RJ, Erkoç E, Dias MM, Teixeira AM, Lopes JCB. Hydrodynamics of the mixing chamber in RIM: PIV flow-field characterization. *AIChE J*. 2008;54(5):1153-1163.

65. Santos RJ, Erkoç E, Dias MM, Lopes JCB. Dynamic behavior of the flow field in a RIM machine mixing chamber. *AIChE J*. 2009;55(6): 1338-1351.

66. Santos RJ, Teixeira AM, Erkoç E, et al. Validation of a 2D CFD model for hydrodynamics' studies in CIJ mixers. *Int J Chem React Eng*. 2010;8.

67. Santos JL, Ren Y, Vandermark J, et al. Continuous production of discrete plasmid DNA-Polycation nanoparticles using flash Nanocomplexation. *Small*. 2016;12(45):6214-6222.

68. Brito MS, Brandão SP, Gonçalves ND, et al. On the control of 2D turbulence by active mixing in opposed jets mixers. *Chem Eng Res Des*. 2023;195:272-285.

69. Fonte CP, Sultan MA, Santos RJ, Dias MM, Lopes JCB. An elastic analog model for controlling the impingement point position in confined impinging jets. *AIChE J*. 2016;62(6):2200-2212.

70. Baldyga J, Bourne JR. Interactions between mixing on various scales in stirred tank reactors. *Chem Eng Sci*. 1992;47(8):1839-1848.

71. Pope SB. *Turbulent Flows*. Cambridge University Press; 2000.

72. Demyanovich RJ, Bourne JR. Rapid micromixing by the impingement of thin liquid sheets. 2. Mixing study. *Ind Eng Chem Res*. 1989;28(6): 830-839.

73. Ottino J, Ranz WE, Macosko CW. A lamellar model for analysis of liquid-liquid mixing. *Chem Eng Sci*. 1979;34(6):877-890.

74. Villermaux J, David R. Recent advances in the understanding of micromixing phenomena in stirred reactors. *Chem Eng Commun*. 1983;21(1-3):105-122.

75. Baldyga J, Bourne JR, Walker B. Non-isothermal micromixing in turbulent liquids: theory and experiment. *Can J Chem Eng*. 1998;76(3): 641-649.

76. Corrsin S. The isotropic turbulent mixer: part II. Arbitrary Schmidt number. *AIChE J*. 1964;10(6):870-877.

77. Webb BW, Ma CF. Single-phase liquid jet impingement heat transfer. *Adv Heat Transf*. 1995;26(C):105-217.

78. Liu WJ, Ma CY, Liu JJ, Zhang Y, Wang XZ. Analytical technology aided optimization and scale-up of impinging jet mixer for reactive crystallization process. *AIChE J*. 2015;61(2):503-517.

79. Unger DR, Muzzio FJ, Brodkey RS. Experimental and numerical characterization of viscous flow and mixing in an impinging jet contactor. *Can J Chem Eng*. 1998;76(3):546-555.

80. Wood P, Hrymak A, Yeo R, Johnson D, Tyagi A. Experimental and computational studies of the fluid mechanics in an opposed jet mixing head. *Phys Fluids A*. 1991;3(5):1362-1368.

81. Johnson DA, Wood PE. Self-sustained oscillations in opposed impinging jets in an enclosure. *Can J Chem Eng*. 2000;78(5):867-875.

82. Hao Y, Seo JH, Hu Y, Mao HQ, Mittal R. Flow physics and mixing quality in a confined impinging jet mixer. *AIP Adv*. 2020;10(4): 045105.

83. Santos RJ. *Mixing Mechanisms in Reaction Injection Moulding: an LDA/PIV Experimental Study and CFD Simulation*. PhD Thesis. Universidade do Porto. 2003.

84. Li W, Du K, Yu G, Liu H, Wang F. Experimental study of flow regimes in three-dimensional confined impinging jets reactor. *AIChE J*. 2014;60(8):3033-3045.

85. Unger DR, Muzzio FJ. Laser-induced fluorescence technique for the quantification of mixing in impinging jets. *AIChE J*. 1999;45(12): 2477-2486.

86. Torres P, Goncalves ND, Fonte CP, et al. Proper orthogonal decomposition and statistical analysis of 2D confined impinging jets chaotic flow. *Chem Eng Technol*. 2019;42(8):1709-1716.

87. Decker HW. Reactive Fluid Mixing Head. US Patent 270,013. 1993.

88. Gomes NMO. *A New Approach for RIM: from RIMCop Technology to Process Design*. PhD Thesis. Universidade do Porto. 2014.

89. Trautmann P, Piesche M. Experimental investigations on the mixing behaviour of impingement mixers for polyurethane production. *Chem Eng Technol*. 2001;24(11):1193-1197.

90. Taubenmann P. Mixing Head for Producing a Preferably Chemically Reactive Mixture of Two or More Plastics Components. US Patent 592,657. 1986.

91. Feng J, Zhang Y, McManus SA, et al. Amorphous nanoparticles by self-assembly: processing for controlled release of hydrophobic molecules. *Soft Matter*. 2019;15(11):2400-2410.

92. Feng J, Markwalter CE, Tian C, Armstrong M, Prudhomme RK. Translational formulation of nanoparticle therapeutics from laboratory discovery to clinical scale. *J Transl Med*. 2019;17(1):1-9.

93. Markwalter CE, Prudhomme RK. Design of a small-scale multi-inlet vortex mixer for scalable nanoparticle production and application to the encapsulation of biologics by inverse flash nanoprecipitation. *J Pharm Sci*. 2018;107(9):2465-2471.

94. Armstrong M, Wang L, Ristroph K, et al. Formulation and scale-up of fast-dissolving Lumefantrine nanoparticles for oral malaria therapy. *J Pharm Sci*. 2023;112(8):2267-2275.

95. Gonçalves ND, Salvador HM, Fonte CP, Dias MM, Lopes JCB, Santos RJ. On the 2D nature of flow dynamics in opposed jets mixers. *AIChE J*. 2017;63(6):2335-2347.

96. Hao Y. *Flow Physics and Mixing of a Confined Impinging Jet Mixer*. PhD Thesis. The John Hopkins University. 2019.

97. Tacsi K, Joo A, Pusztai E, et al. Development of a triple impinging jet mixer for continuous antisolvent crystallization of acetylsalicylic acid reaction mixture. *Chem Eng Process Process Intens*. 2020;2021(165): 1-11.

98. Lince F, Marchisio DL, Barresi AA. Smart mixers and reactors for the production of pharmaceutical nanoparticles: proof of concept. *Chem Eng Res Des*. 2009;87(4):543-549.

99. Yang L, Xu F, Chen G. Effective mixing in a passive oscillating micromixer with impinging jets. *Chem Eng J*. 2024;489:151329.

100. Lindrud DM, Kim S, Chenkou W. Sonic Impinging Jet Crystallization Apparatus and Process. US Patent 6,302,958 B1. 2001.

101. Siddiqui SW, Wan Mohamad WA, Mohd Rozi MF, Norton IT. Continuous, high-throughput flash-synthesis of submicron food emulsions using a confined impinging jet mixer: effect of in situ turbulence, sonication, and small surfactants. *Ind Eng Chem Res*. 2017;56(44):12833-12847.

102. Siddiqui SW, Unwin PJ, Xu Z, Kresta SM. The effect of stabilizer addition and sonication on nanoparticle agglomeration in a confined impinging jet reactor. *Colloids Surf A Physicochem Eng Asp*. 2009; 350(1-3):38-50.

103. Teixeira AM, Santos RJ, Costa MRP, Lopes JCB. Hydrodynamics of the mixing head in RIM: LDA flow-field characterization. *AIChE J*. 2005;51(6):1608-1619.

104. Shi Z, wf L, Du Kj LH, Fc W. Experimental study of mixing enhancement of viscous liquids in confined impinging jets reactor at low jet Reynolds numbers. *Chem Eng Sci*. 2015;138:216-226.

105. Baldyga J, Bourne JR, Gholap RV. The influence of viscosity on mixing in jet reactors. *Chem Eng Sci*. 1995;50(12):1877-1880.

106. Ashar Sultan M, Fonte CP, Dias MM, Lopes JCB, Santos RJ. Experimental study of flow regime and mixing in T-jets mixers. *Chem Eng Sci*. 2012;73:388-399.

107. Bourne JR, Maire H. Micromixing and fast chemical reactions in static mixers. *Chem Eng Process*. 1991;30(1):23-30.

108. Valdés JP, Kahouadji L, Matar OK. Current advances in liquid-liquid mixing in static mixers: a review. *Chem Eng Res Des*. 2022;177(29):694-731.

109. Ghanem A, Lemenand T, Della Valle D, Peerhossaini H. Static mixers: mechanisms, applications, and characterization methods – a review. *Chem Eng Res Des*. 2014;92(2):205-228.

110. Nguyen NT, Wu Z. Micromixers – a review. *J Micromech Microeng*. 2005;15(2):R1-R16.

111. Thakur RK, Vial C, Nigam KD, Nauman EB, Djelveh G. Static mixers in the process industries – a review. *Chem Eng Res Des*. 2003;81(7):787-826.

112. Bayareh M, Ashani MN, Usefian A. Active and passive micromixers: a comprehensive review. *Chem Eng Process Process Intens*. 2020;147:107771.

113. Falk L, Commenge JM. Performance comparison of micromixers. *Chem Eng Sci*. 2010;65(1):405-411.

114. Hessel V, Löwe H, Schönfeld F. Micromixers – a review on passive and active mixing principles. *Chem Eng Sci*. 2005;60(8-9):2479-2501.

115. Schwertfirm F, Gradl J, Schwarzer HC, Peukert W, Manhart M. The low Reynolds number turbulent flow and mixing in a confined impinging jet reactor. *Int J Heat Fluid Flow*. 2007;28(6):1429-1442.

116. Bertsch A, Bongarzone A, Duchamp M, Renaud P, Gallaire F. Feedback-free microfluidic oscillator with impinging jets. *Phys Rev Fluid*. 2020;5(5):54202.

117. Bénet N, Falk L, Muhr H, Plasari E. Characterisation and modelling of a two impinging jet mixer for precipitation processes using laser induced fluorescence. *10th European Conference on Mixing*. ScienceDirect; 2000:35-44.

118. Danckwerts PV. The definition and measurement of some characteristics of mixtures. *Appl Sci Res Sec A*. 1952;3(4):279-296.

119. Gao Z, Han J, Xu Y, Bao Y, Li Z. Particle image velocimetry (PIV) investigation of flow characteristics in confined impinging jet reactors. *Ind Eng Chem Res*. 2013;52(33):11779-11786.

120. Bourne JR, Kozicki F, Rys P. Mixing and fast chemical reaction—I. *Chem Eng Sci*. 1981;36(10):1643-1648.

121. Commenge J, Falk L. Villermaux-Dushman protocol for experimental characterization of micromixers. *Chem Eng Process Process Intensif*. 2011;50(10):979-990.

122. Lemenand T, Della Valle D, Habchi C, Peerhossaini H. Micro-mixing measurement by chemical probe in homogeneous and isotropic turbulence. *Chem Eng J*. 2017;314:453-465.

123. Fournier M, Falk L, Villermaux J. Assessing micromixing efficiency–determination of micromixing time by a simple mixing. *Chem Eng Sci*. 1996;51(23):5187-5192.

124. Fournier MC, Falk L, Villermaux J. A new parallel competing reaction system for assessing micromixing efficiency – experimental approach. *Chem Eng Sci*. 1996;51(22):5053-5064.

125. Wenzel D, Górak A. Review and analysis of micromixing in rotating packed beds. *Chem Eng J*. 2017;2018(345):492-506.

126. Bourne JR, Kut OM, Lenzner J. An improved reaction system to investigate micromixing in high-intensity mixers. *Ind Eng Chem Res*. 1992;31(3):949-958.

127. Abiev RS, Sirotkin AA. Effect of hydrodynamic conditions on micro-mixing in impinging-jets microreactors. *Theor Found Chem Eng*. 2022;56(1):9-22.

128. Siddiqui SW, Zhao Y, Kukukova A, Kresta SM. Characteristics of a confined impinging jet reactor: energy dissipation, homogeneous and heterogeneous reaction products, and effect of unequal flow. *Ind Eng Chem Res*. 2009;48(17):7945-7958.

129. Jaramillo JE, Trias FX, Gorobets A, Prez-Segarra CD, Oliva A. DNS and RANS modelling of a turbulent plane impinging jet. *Int J Heat Mass Transf*. 2012;55(4):789-801.

130. Eswaran V, Pope SB. An examination of forcing in direct numerical simulations of turbulence. *Comput Fluids*. 1988;16(3):257-278.

131. Juneja A, Pope SB. A DNS study of turbulent mixing of two passive scalars. *Phys Fluids*. 1996;8(8):2161-2184.

132. Fox RO. *Computational Models for Turbulent Reacting Flows*. Cambridge University Press; 2003.

133. Wilcox DC. *Turbulence Modelling for CFD*. 3rd ed. DCW Industries; 2006.

134. Speziale CG, Sarkar S, Gatski TB. Modelling the pressure-strain correlation of turbulence: an invariant dynamical systems approach. *J Fluid Mech*. 1991;227:245-272.

135. Launder BE, Reece GJ, Rodi W. Progress in the development of a Reynolds-stress turbulence closure. *J Fluid Mech*. 1975;68(3):537-566.

136. Hellsten A. Some improvements in Menter's k-omega SST turbulence model. *29th AIAA, Fluid Dynamics Conference*. American Institute of Aeronautics and Astronautics; 1998.

137. Madadi-Kandjani E, Passalacqua A, Fox RO. Investigation of the mixing inside the confined impinging jet mixer using the Fokker-Planck mixing model. *Chem Eng Sci*. 2023;273:118634.

138. Smagorinsky J. General circulation experiments with the primitive equations. *Mon Weather Rev*. 1963;91(3):99-164.

139. Mason PJ. Large-eddy simulation: a critical review of the technique. *Q J R Meteorol Soc*. 1994;120(515):1-26.

140. Germano M, Piomelli U, Moin P, Cabot WH. A dynamic subgrid-scale eddy viscosity model. *Phys Fluids A Fluid Dyn*. 1991;3(7):1760-1765.

141. Michioka T, Komori S. Large-eddy simulation of a turbulent reacting liquid flow. *AIChE J*. 2004;50(11):2705-2720.

142. Makowski L, Bałdyga J. Large Eddy simulation of mixing effects on the course of parallel chemical reactions and comparison with k-e modeling. *Chem Eng Process Process Intensif*. 2011;50(10):1035-1040.

143. Madadi-Kandjani E, Fox RO, Passalacqua A. Application of the Fokker-Planck molecular mixing model to turbulent scalar mixing using moment methods. *Phys Fluids*. 2017;29(6):065109.

144. Combest DP, Ramachandran PA, Dudukovic MP. On the gradient diffusion hypothesis and passive scalar transport in turbulent flows. *Ind Eng Chem Res*. 2011;50(15):8817-8823.

145. Baldyga J, Bourne JR. Comparison of the engulfment and the interaction-by-exchange-with-the-mean micromixing models. *Chem Eng J*. 1990;45(1):25-31.

146. Akroyd J, Smith AJ, McGlashan LR, Kraft M. Numerical investigation of DQMoM-IEM as a turbulent reaction closure. *Chem Eng Sci*. 2010;65(6):1915-1924.

147. Fox RO. The Fokker-Planck closure for turbulent molecular mixing: passive scalars. *Phys Fluid A Fluid Dyn*. 1992;4(6):1230-1244.

148. Fox RO. On the relationship between Lagrangian micromixing models and computational fluid dynamics. *Chem Eng Process Process Intensif*. 1998;37(6):521-535.

149. Pope SB, Lagrangian PDF. Methods for turbulent flows. *Annu Rev Fluid Mech*. 1994;26(1):23-63.

150. Wang L, Fox RO. Comparison of micromixing models for CFD simulation of nanoparticle formation. *AIChE J*. 2004;50(9):2217-2232.

151. Marchisio DL, Barresi AA, Garbero M. Nucleation, growth, and agglomeration in barium sulfate turbulent precipitation. *AIChE J*. 2002;48(9):2039-2050.

152. Fan R, Marchisio DL, Fox RO. Application of the direct quadrature method of moments to polydisperse gas-solid fluidized beds. *Powder Technol*. 2004;139(1):7-20.

153. Liu Z, Hitimana E, Olsen MG, Hill JC, Fox RO. Turbulent mixing in the confined swirling flow of a multi-inlet vortex reactor. *AIChE J*. 2017;63(6):2409-2419.

154. Bakosi J, Franzese P, Boybeyi Z. Probability density function modeling of scalar mixing from concentrated sources in turbulent channel flow. *Phys Fluids*. 2007;19(11):115106.

155. Ramkrishna D, Singh MR. Population balance modeling: current status and future prospects. *Annu Rev Chem Biomol Eng*. 2014;5(1):123-146.

156. Martin H. Heat and mass transfer between impinging gas jets and solid surfaces. *Advances in Heat Transfer*. Vol 13. Elsevier; 1977:1-60.

157. Phares DJ, Smedley GT, Flagan RC. The inviscid impingement of a jet with arbitrary velocity profile. *Phys Fluids*. 2000;12(8):2046-2055.

158. Donaldson CP, Snedeker RS. A study of free jet impingement. Part 1. Mean properties of free and impinging jets. *J Fluid Mech*. 1971;45(2):281-319.

159. Deen WM. *Analysis of Transport Phenomena*. 1st ed. Oxford University Press; 1998.

160. Jiang M, Gu C, Braatz RD. Understanding temperature-induced primary nucleation in dual impinging jet mixers. *Chem Eng Process Process Intensif*. 2015;97:187-194.

161. Wu Y. *Impinging Streams: Fundamentals, Properties and Applications*. 1st ed. Elsevier; 2007.

162. Powell A. Aerodynamic noise and the plane boundary. *J Acoust Soc Am*. 1960;32(8):982-990.

163. Nosseir N, Peled U, Hildebrand G. Pressure field generated by jet-on-jet impingement. *AIAA J*. 1987;25(10):1312-1317.

164. Boyce WE, DiPrima RC. *Elementary Differential Equations*. Vol 6. Wiley; 2012.

165. Singh S, Murthy P. Significance of skewness and kurtosis on the solute dispersion in pulsatile Carreau–Yasuda fluid flow in a tube with wall absorption. *J Fluid Mech*. 2023;962:A42.

166. Fonte CP, Santos RJ, Dias MM, Lopes JCB. Quantification of mixing in RIM using a non-diffusive two-phase flow numerical model. *Int J Chem Reactor Eng*. 2011;9.

167. Krupa K, Sultan MA, Fonte CP, et al. Characterization of mixing in T-jets mixers. *Chem Eng J*. 2012;207-208:931-937.

168. Zhang JW, Li WF, Xu XL, El Hassan M, Liu HF, Wang FC. Effect of geometry on engulfment flow regime in T-jet reactors. *Chem Eng J*. 2020;387(September 2019):124148.

169. Soleymani A, Yousefi H, Turunen I. Dimensionless number for identification of flow patterns inside a T-micromixer. *Chem Eng Sci*. 2008;63(21):5291-5297.

170. Li H, Xu D. An overview of fluids mixing in T-shaped mixers. *Theor Appl Mech Lett*. 2023;13(4):100466.

171. Brito MS, Fonte CP, Dias MM, Lopes JCB, Santos RJ. Flow regimes and mixing of dissimilar fluids in T-jets mixers. *Chem Eng Technol*. 2022;45(2):355-364.

172. Bothe D, Stemich C, Warnecke HJ. Fluid mixing in a T-shaped micro-mixer. *Chem Eng Sci*. 2006;61(9):2950-2958.

173. Denshchikov VA, Kondrat VN, Romashov AN, Chubarov VM. Auto-oscillations of planar colliding jets. *Fluid Dyn*. 1983;18(3):460-462.

174. Denshchikov VA, Kondrat'ev VN, Romashov AN. Interaction between two opposed jets. *Fluid Dyn*. 1979;13(6):924-926.

175. Li X, Santos RJ, Lopes JCB. Modelling of self-induced oscillations in the mixing head of a RIM machine. *Can J Chem Eng*. 2007;85(1):45-54.

176. Rockwell D. Oscillations of impinging shear layers. *AIAA J*. 1983;21(5):645-664.

177. Li W, Qian W, Yu G, Liu H, Wang F. Experimental study of oscillation behaviors in confined impinging jets reactor under excitation. *AIChE J*. 2015;61(1):333-341.

178. Li W, Yao T, Liu H, Wang F. Experimental investigation of flow regimes of axisymmetric and planar opposed jets. *AIChE J*. 2011;57(6):1434-1445.

179. Li W, Yao T, Wang F. Study on factors influencing stagnation point offset of turbulent opposed jets. *AIChE J*. 2010;56(10):2513-2522.

180. O'Neill P, Soria J, Honnery D. The stability of low Reynolds number round jets. *Exp Fluid*. 2004;36(3):473-483.

181. Gy T, Li Wf D, Kj WF. Experimental investigation of deflecting oscillation in T-jets reactor. *Chem Eng Sci*. 2014;116:734-744.

182. Boffetta G, Ecke RE. Two-dimensional turbulence. *Annu Rev Fluid Mech*. 2011;44:427-451.

183. Xiao Z, Wan M, Chen S, Eyink GL. Physical mechanism of the inverse energy cascade of two-dimensional turbulence: a numerical investigation. *J Fluid Mech*. 2009;619:1-44.

184. Hu Y, He Z, Hao Y, et al. Kinetic control in assembly of plasmid DNA/polycation complex nanoparticles. *ACS Nano*. 2019;13(9):10161-10178.

185. Tripodi E, Norton IT, Spyropoulos F. Formation of pickering and mixed emulsifier systems stabilised O/W emulsions via confined impinging jets processing. *Food Bioprod Process*. 2020;119:360-370.

186. May HO. A field equation for the distribution of striation thickness from impingement mixers. *Polym Eng Sci*. 1996;36(4):583-585.

187. Fonte D. *Mixing Studies with Impinging Jets*. PhD Thesis. Universidade do Porto. 2012.

188. Khan MS, Mane M, Kulkarni AA. Evaluating suitability of confined impinging jet reactor for exothermic reactions: hydrodynamics, residence time distribution, and heat transfer. *AIChE J*. 2022;68(10):1-16.

189. Ji L, Wu B, Chen K, Zhu J. Experimental study and modeling of residence time distribution in impinging stream reactor with GDB model. *J Ind Eng Chem*. 2010;16(4):646-650.

190. Liu WJ, Ma CY, Wang XZ. Novel impinging jet and continuous crystallizer design for rapid reactive crystallization of pharmaceuticals. *Proc Eng*. 2015;102:499-507.

191. Lee LJ. Reaction injection molding. *Comprehensive Polymer Science and Supplements*. Elsevier; 1989:379-426.

192. Fields SD, Ottino JM. Effect of striation thickness distribution on the course of an unpremixed polymerization. *Chem Eng Sci*. 1987;42(3):459-465.

193. Saien J, Ebrahimzadeh Zonouzian SA, Dehkordi AM. Investigation of a two impinging-jets contacting device for liquid-liquid extraction processes. *Chem Eng Sci*. 2006;61(12):3942-3950.

194. Tsaoulidis D, Ortega EG, Angeli P. Intensified extraction of uranium(VI) in impinging-jets contactors. *Chem Eng J*. 2018;342(Feb):251-259.

195. Dehkordi AM. Novel type of impinging streams contactor for liquid-liquid extraction. *Ind Eng Chem Res*. 2001;40(2):681-688.

196. Saien J, Doghahe SAO, Dehkordi AM. Retarding effect of contaminants on the performance of a two-impinging-jets liquid-liquid extraction contactor. *Chem Eng Technol*. 2010;33(6):1003-1010.

197. Tsaoulidis D, Angeli P. Liquid-liquid dispersions in intensified impinging-jets cells. *Chem Eng Sci*. 2017;171:149-159.

198. Siddiqui SW. The effect of oils, low molecular weight emulsifiers and hydrodynamics on oil-in-water emulsification in confined impinging jet mixer. *Colloids Surf A Physicochem Eng Asp*. 2014;443:8-18.

199. Siddiqui SW, Norton IT. Oil-in-water emulsification using confined impinging jets. *J Colloid Interface Sci*. 2012;377(1):213-221.

200. Ho TM, Razzaghi A, Ramachandran A, Mikkonen KS. Emulsion characterization via microfluidic devices: a review on interfacial tension and stability to coalescence. *Adv Colloid Interface Sci*. 2021;2022(299):102541.

201. Saien J, Moradi V. Low interfacial tension liquid-liquid extraction with impinging-jets contacting method: influencing parameters and relationship. *J Ind Eng Chem*. 2012;18(4):1293-1300.

202. Saien J, Ojaghi SA. Effect of aqueous phase pH on liquid-liquid extraction with impinging-jets contacting technique. *J Ind Eng Chem*. 2010;16(6):1001-1005.

203. Gao Z, Zhao M, Yu Y, Li Z, Han J. Investigation of extraction fraction in confined impinging jet reactors for tri-butyl-phosphate extracting butyric acid process. *Chin J Chem Eng*. 2016;24(2):310-316.

204. Woo XY, Tan RBH, Braatz RD. Modeling and computational fluid dynamics – population balance equation – micromixing simulation of impinging jet crystallizers. *Cryst Growth Des*. 2009;9(1):156-164.

205. Roelands CPM, ter Horst JH, Kramer HJM, Jansens PJ. Analysis of nucleation rate measurements in precipitation processes. *Cryst Growth Des*. 2006;6(6):1380-1392.

206. Wang H, Mustaffar A, Phan AN, et al. A review of process intensification applied to solids handling. *Chem Eng Process Process Intensif*. 2017;118:78-107.

207. Adavi K, Dehkordi AM. Synthesis and polymorph controlling of calcite and aragonite calcium carbonate nanoparticles in a confined impinging-jets reactor. *Chem Eng Process Process Intens*. 2021;159:108239.

208. Midler MJ, Paul EL, Whittington E, Liu P, Hsu J, Pan S. Crystallization Method to Improve Crystal Structure and Size. US Patent 314,506. 1994.

209. Dauer R, Mokrauer JE, McKeel WJ. Dual Jet Crystallizer Apparatus. US Patent 5,578,279. 1996.

210. Da Rosa CA, Braatz RD. Multiscale modeling and simulation of macromixing, micromixing, and crystal size distribution in radial mixers/crystallizers. *Ind Eng Chem Res*. 2018;57(15):5433-5441.

211. Am Ende DJ, Crawford TC, Weston NP. Reactive Crystallization Method to Improve Particle Size. US Patent 6,558,435 B2. 2003.

212. D'Addio SM, Prudhomme RK. Controlling drug nanoparticle formation by rapid precipitation. *Adv Drug Deliv Rev*. 2011;63(6):417-426.

213. Inguva P, Grasselli S, Heng PW. High pressure homogenization – an update on its usage and understanding. *Chem Eng Res Des*. 2024;202:284-302.

214. Chan HK, Kwok PCL. Production methods for nanodrug particles using the bottom-up approach. *Adv Drug Deliv Rev*. 2011;63(6):406-416.

215. Stelzer T, Lakerveld R, Myerson AS. Process intensification in continuous crystallization. *The Handbook of Continuous Crystallization*. The Royal Society of Chemistry; 2020:266-320.

216. Zhao P, Tian Y, You J, Hu X, Liu Y. Recent advances of calcium carbonate nanoparticles for biomedical applications. *Bioengineering*. 2022;9(11):691.

217. Albadi Y, Abiev R, Sirotkin A, et al. Physicochemical and hydrodynamic aspects of GdFeO3 production using a free impinging-jets method. *Chem Eng Process Process Intens*. 2021;166:108473.

218. Baber R, Mazzei L, Thanh NT, Gavriilidis A. Synthesis of silver nanoparticles using a microfluidic impinging jet reactor. *J Flow Chem*. 2016;6(3):268-278.

219. Sahoo K, Kumar S. Green synthesis of sub 10 nm silver nanoparticles in gram scale using free impinging jet reactor. *Chem Eng Process Process Intensif*. 2021;165:108439.

220. Xu L, Srinivasakannan C, Peng J, Zhang D, Chen G. Synthesis of nickel nanoparticles by aqueous reduction in continuous flow microreactor. *Chem Eng Process Process Intensif*. 2015;93:44-49.

221. Kügler RT, Kind M. Experimental study about plugging in confined impinging jet mixers during the precipitation of strontium sulfate. *Chem Eng Process Process Intensif*. 2016;101:25-32.

222. Kügler RT, Doyle S, Kind M. Fundamental insights into barium sulfate precipitation by time-resolved in situ synchrotron radiation wide-angle X-ray scattering (WAXS). *Chem Eng Sci*. 2015;133:140-147.

223. Gavi E, Rivautella L, Marchisio D, Vanni M, Barresi A, Baldi G. CFD modelling of nano-particle precipitation in confined impinging jet reactors. *Chem Eng Res Des*. 2007;85(5):735-744.

224. Heger R, Auweter H, Breitenbach J, Bohn H. Nanoparticulate Core Shell Systems and the Use Thereof in Pharmaceutical and Cosmetic Preparation. Canadian Patent 2353809A1. 2010.

225. Mao HQ, Santos JL, Ren Y, Williford JM. Methods of Preparing Poly-Electrolyte Complex Nanoparticles. US Patent 11,395,805 B2. 2022.

226. Prudhomme RK, Gindy ME, Liu Y. Composite Flash-Precipitated Nanoparticles. US Patent 2018 US2018/0243229 A1. 2022.

227. Smith M, Horhota A, Auer J, Skinner B. Methods of Preparing Lipid Nanoparticles. International Patent WO 2020/160397. 2020.

228. Johnson BK, Prudhomme RK. Process and Apparatuses for Preparing Nanoparticle Compositions With Amphiphilic Copolymers And Their Use. US Patent 9,956,179 B2. 2018.

229. Lee VE, Scott DM, Prudhomme RK, Priestley RD. Flash Nano-precipitation and -complexation to produce polymer colloids. *Polymer Colloids: Formation, Characterization and Applications*. The Royal Society of Chemistry; 2019:61-99.

230. Hu H, Yang C, Li M, Shao D, Mao HQ, Leong KW. Flash technology-based self-assembly in nanoformulation: fabrication to biomedical applications. *Mater Today*. 2021;42:99-116.

231. Thorn CR, Sharma D, Combs R, et al. The journey of a lifetime — development of Pfizer's COVID-19 vaccine. *Curr Opin Biotechnol*. 2022;78:102803.

232. Johnson ID, Lübke M, Wu OY, et al. Pilot-scale continuous synthesis of a vanadium-doped LiFePO4/C nanocomposite high-rate cathodes for lithium-ion batteries. *J Power Sources*. 2016;302:410-418.

233. Tan Z, Luo X, Wei T, et al. In situ formation of NiAl-layered double hydroxide with a tunable interlayer spacing in a confined impinging jet microreactor. *Energy Fuel*. 2020;34(7):8939-8946.

234. Bojarska Z, Mazurkiewicz-Pawlicka M, Mierzwa B, Ploci ML. Effect of the carbon support on MoS2 hybrid nanostructures prepared by an impinging jet reactor for hydrogen evolution reaction catalysis. *J Environ Chem Eng*. 2022;10(4):108038.

235. Lee VE, Sosa C, Liu R, Prud RK, Priestley RD. Scalable platform for structured and hybrid soft nanocolloids by continuous precipitation in a confined environment. *Langmuir*. 2017;33(14):3444-3449.

236. Kang C, Honciuc A. Versatile triblock Janus nanoparticles: synthesis and self-assembly. *Chem Mater*. 2019;31(5):1688-1695.

237. Zhang Q, Gamekkanda JC, Pandit A, et al. Extracting particle size distribution from laser speckle with a physics-enhanced autocorrelation-based estimator (PEACE). *Nat Commun*. 2023;14(1):1-9.

238. Banu KS, Lerma M, Ahmed SU, Gardea-Torresdey JL. Hyperspectral microscopy- applications of hyperspectral imaging techniques in different fields of science: a review of recent advances. *Appl Spectrosc Rev*. 2023;59(7):935-938.

239. Harley JL, Rankin BA, Blunck DL, Gore JP, Gross KC. Imaging Fourier-transform spectrometer measurements of a turbulent non-premixed jet flame. *Opt Lett*. 2014;39(8):2350.

240. Pfizer. Breakthrough vaccine to potentially protect against the spread of COVID-19. Technical Report. 2020.

241. Guray T. A study of micromixing in tee mixers. *Ind Eng Chem Res*. 1987;26:1184-1193.

242. Demyanovich RJ. Production of commercial dyes via impingement-sheet mixing. Part I. Testing of a device suitable for industrial application. *Chem Eng Process*. 1991;29(3):173-177.

243. Bourne JR, Lenzner J, Petrozzi S. Micromixing in static mixers: an experimental study. *Ind Eng Chem Res*. 1992;31(4):1216-1222.

244. Bourne JR, Studer M. Fast reactions in rotor-stator mixers of different size. *Chem Eng Process*. 1992;31(5):285-296.